Ecological Modelling 445 (2021) 109492

Contents lists available at ScienceDirect

Ecological Modelling

journal homepage: www.elsevier.com/locate/ecolmodel

Improved estimation of gross primary production of paddy rice cropland with changing model parameters over phenological transitions

Duan Huang[a,b], Hong Chi[b,c,*], Fengfei Xin[d], Akira Miyata[e], Minseok Kang[f], Kaiwen Liu[g], Rendong Li[b], Haishan Dang[h], Yuanwei Qin[c], Xiangming Xiao[c]

[a] *Faculty of Geomatics, East China University of Technology, Nanchang, Jiangxi 330013, China*
[b] *Key laboratory for Environment and Disaster Monitoring and Evaluation, Innovation Academy for Precision Measurement Science and Technology, Chinese Academy of Sciences, Wuhan, Hubei 430077, China*
[c] *Department of Microbiology and Plant Biology, Center for Spatial Analysis, University of Oklahoma, Norman, OK 73019, United States*
[d] *Ministry of Education Key Laboratory of Biodiversity Science and Ecological Engineering, Institute of Biodiversity Science, Fudan University, Shanghai 200433, China*
[e] *NARO, Institute for Agro-Environmental Science, Tsukuba, 305-8604, Japan*
[f] *National Center for AgroMeteorology, Seoul 08826, Republic of Korea*
[g] *Jingzhou Agriculture Meteorological Trial Station, Jingzhou, Hubei 434025, China*
[h] *Key Laboratory of Aquatic Botany and Watershed Ecology, Wuhan Botanical Garden, Chinese Academy of Sciences, Wuhan, 430074 China*

A R T I C L E I N F O

Keywords:
Maximum light-use efficiency
Optimum temperature
Gross primary production
Vegetation photosynthesis model
CO_2 fluxes
Paddy rice phenology

A B S T R A C T

Paddy rice is one of the main grain crops in the world. Accurate estimations of the gross primary production (GPP) of paddy rice are essential for assessing rice grain production and monitoring the carbon cycle in paddy fields with the aim of providing ideal conditions for crops throughout the growing season. Several studies have demonstrated the advantages of combining the eddy covariance technique with remotely sensed data to model GPP at CO_2 eddy flux tower sites. As paddy rice continuously changes during its growth and development, and important growth events frequently occur, it is critical to observe the growing conditions at various stages of the process. To better understand the variations in GPP at different growth stages, two key parameters that drive the vegetation photosynthesis model (VPM) are analyzed and estimated at various phenological phases. Specifically, general piecewise logistic functions are used to extract phenological transitions from data at four paddy rice flux tower sites. The maximum light-use efficiency (LUE) and optimum temperature are estimated from these phenological transitions, and these indicators are used to drive the VPM to simulate GPP over multiple years at the four sites. The simulation results show that GPP based on our phenological transition-based VPM (GPP_{PVPM}) agrees reasonably well with the variations of GPP estimated from CO_2 flux data (GPP_{EC}) ($R^2 > 0.9$). In addition, a comparison indicates that GPP_{PVPM} tracks the seasonal dynamics of GPP_{EC} better than GPP estimated from the original VPM. Furthermore, GPP based on the improved maximum LUE is lower than GPP_{EC} at most flux sites and GPP based on the improved optimum temperature is higher than GPP_{EC}. These comparisons imply that the maximum LUE and optimum temperature estimated in the phenological transitions of paddy rice are beneficial to enhance the accuracy of GPP estimation. The improved estimation of GPP provides phenological insights into the temporal dynamics of vegetation photosynthesis in paddy fields.

1. Introduction

Paddy rice fields are among the major global agricultural ecosystems, and were estimated to cover approximately 167 million hectares worldwide in 2017 (FAOSTAT, 2017). The majority of the world's paddy fields are in Asia, accounting for approximately 87% of the globally harvested rice area and 90% of global rice production (FAOSTAT, 2017). Irrigated rice fields are also one of the major sources of methane (CH_4), as the inherent anaerobic soil conditions are conducive to methane production (Neue, 1993). Although several in-situ studies have reported that paddy rice fields enable high levels of carbon sequestration and act as net sinks for carbon dioxide (CO_2) (Bhattacharyya et al., 2014; Liu et al., 2013; Pan et al., 2004), predictions of the carbon fluxes in paddy rice fields suffer from considerable uncertainties (Xin et al., 2017). The

* Corresponding author.
E-mail address: chihong@whigg.ac.cn (H. Chi).

https://doi.org/10.1016/j.ecolmodel.2021.109492
Received 25 June 2020; Received in revised form 10 February 2021; Accepted 13 February 2021
Available online 1 March 2021

exchange of CO_2 between agricultural ecosystems and the atmosphere plays an important role in the carbon cycle. The amount of CO_2 fixed from radiant energy absorbed by the paddy rice field is strongly related to the physiological and phenological activities of croplands (Hanan et al., 2002). Therefore, the measurement of CO_2 fluxes in paddy rice fields is crucial in clarifying the physiological responses of crops to environmental conditions. Furthermore, a better understanding of this process will be beneficial for the prediction of grain production under climate change conditions.

The gross primary production (GPP) of paddy rice reflects the CO_2 flux fixed by crops through the process of photosynthesis, and is the main variable determining crop yield. The eddy covariance (EC) technique is one of the best micrometeorological methods for measuring the net exchange of CO_2 between the atmosphere and the surface of various ecosystems. The observed net ecosystem exchange (NEE) data can be partitioned into GPP and ecosystem respiration (denoted as R_e) (Baldocchi et al., 2001). These NEE data and the derived GPP and R_e data from flux sites have been widely used to support the development of GPP simulation models for satellite remote sensing and climate data at regional and global scales (Running et al., 1999; Stockli et al., 2008; Williams et al., 2009). EC flux measurements from global flux networks provide valuable information for calibrating and validating the parameters of these models in an attempt to improve the GPP estimation capability, facilitating numerous studies of carbon fluxes over paddy rice ecosystems (Alberto et al., 2009; Baldocchi et al., 2001; Choi et al., 2018; Hwang et al., 2020; Knox et al., 2015; Saito et al., 2005; Xin et al., 2017).

Light-use efficiency (LUE) models have significant potential to address the spatial and temporal dynamics of GPP, because they take advantage of extensive satellite observations (Yuan et al., 2014; Zhang et al., 2017). These satellite-based models assume that the GPP of a terrestrial ecosystem is directly related to the absorbed photosynthetically active radiation (APAR) through LUE (Monteith, 1972, 1977), and have been developed to estimate the GPP of terrestrial ecosystems through vegetation indices (VIs) derived from remotely sensed optical images and meteorological data (Barton and North, 2001; Brogaard et al., 2005; Machwitz et al., 2015; Nichol et al., 2000; Potter et al., 1993; Yuan et al., 2007). The GPP estimated from these models is the product of APAR and the LUE (denoted as ε_g), i.e., GPP = APAR × ε_g. Earlier studies using LUE models employed the fraction of photosynthetically active radiation (PAR) absorbed by the vegetation canopy ($FPAR_{canopy}$) to estimate $APAR_{canopy}$ = PAR × FPAR, where $FPAR_{canopy}$ was approximated using VIs (Potter et al., 1993; Zhao et al., 2005). For example, the MOD17 product employs MOD15A2 FPAR, which is a canopy-level FPAR comprised of both photosynthetic and non-photosynthetic components (Cheng et al., 2014; Zhang et al., 2014). As the fraction of PAR absorbed by chlorophyll ($FPAR_{chl}$) contributes to vegetation photosynthesis, it is more reasonable to use $FPAR_{chl}$ to estimate GPP = PAR × $FPAR_{chl}$ × ε_g (Sims et al., 2006; Wu et al., 2010; Xiao et al., 2004b; Zhang et al., 2009, 2006). The vegetation photosynthesis model (VPM) was the first LUE-based model to use $FPAR_{chl}$ to estimate GPP (Xiao et al., 2004a). Previous research has shown the comprehensive ability of VPM to estimate GPP over a variety of CO_2 flux sites (Wu et al., 2018), including forests (Xiao et al., 2004a, 2004b, 2005a; Xiao et al., 2005b), savanna (Jin et al., 2013), grassland (Wang et al., 2010; Yang et al., 2019), and cropland (Ma et al., 2020; Wang et al., 2010). Recently, VPM has been successfully applied to the estimation of GPP in paddy rice fields (Xin et al., 2017).

In VPM, the actual LUE (ε_g) may be less than its theoretical maximum because of environmental stresses such as extreme temperatures, water shortages, or flooding. Therefore, ε_g is determined by the maximum LUE (ε_0) and a water stress factor (W_{scalar}), as well as a temperature stress factor (T_{scalar}), i.e., $\varepsilon_g = \varepsilon_0 \times T_{scalar} \times W_{scalar}$. In most research on paddy rice GPP estimation using VPM, the ecosystem-level $\varepsilon_0$can be obtained from analysis of the NEE of CO_2 and the incident PAR (μmol/m^2/s) at CO_2 eddy flux sites, either by using the hyperbolic light response function (Alberto et al., 2009; Inoue et al., 2008; Lindner et al., 2016; Saito et al., 2005; Yang et al., 2018) or by taking a suitable value from the literature (Xin et al., 2017; Yan et al., 2009). The ε_0 estimates given by the former approach are based on analyses of half-hourly NEE and incident PAR data, either by dividing the entire growing season into several growth periods (Saito et al., 2005) or by considering the entire growing season at the flux sites (Alberto et al., 2009). Some photosynthesis research has demonstrated that, within C_3 species, annual herbaceous plants (e.g., paddy rice) display weaker temperature homeostasis of photosynthesis than perennial herbaceous plants (e.g., wheat) (Yamori et al., 2014). More importantly, the growth and development of paddy rice plants involve continuous change, which means that important growth events occur frequently. Therefore, the overall daily or healthy growth stages of the plant are crucial. To better understand the development of paddy rice and properly manage the rice crop, it is essential to separate the entire growing season of paddy rice into individual growing seasons according to physiological and phenological characteristics for ε_0 estimation. Moreover, the effect of temperature stress (T_{scalar}) is an uncertain factor in LUE models due to the relationship between temperature and photosynthesis. Few scholars have focused on the temperature stress factors. In VPM, T_{scalar} is determined by two temperature factors, T_{min} and T_{max}. The basic hypothesis behind T_{min} and T_{max} is that vegetation growth acclimatizes to the optimum temperature (T_{opt}), which is defined as the mean temperature of the month when the normalized difference vegetation index (NDVI) reaches its maximum (Field et al., 1995; Potter et al., 1993), or the average temperature of the growth season (Yan et al., 2009). However, this definition may not be comprehensive for the following reasons: (1) in cropland ecosystems, the growing seasons of crops span several physiological stages, and the use of a uniform average temperature in the growing season, either site-specific or on a regional scale, needs to be improved; (2) due to extreme weather events or natural disasters, the maximum NDVI or enhanced vegetation index (EVI) values in some areas may not occur in July or August, as typically expected; and (3) abnormal maximum NDVI or EVI values may occur for other reasons. Recent work has shown that improvements in phenology-based research on optimum temperatures significantly enhances forest net primary production (NPP) estimations using the Carnegie–Ames–Stanford Approach (CASA) model (Pei et al., 2018). However, this approach has not yet been applied to estimations of the GPP of crop ecosystems.

To overcome uncertainties in the determination of the maximum LUE (ε_0) of paddy rice fields and the limitations of the definition of optimum temperature in the LUE model, this research first attempts to understand and estimate the model parameters (ε_0 and optimum temperature) at various phenological phases, and then generates improved GPP estimations by running VPM with parameters that are appropriate for the individual phenological phases. The results of this work are expected to make a significant contribution in terms of improving the accuracy of GPP estimation and promoting our long-term monitoring capabilities in rice agriculture, which feeds more than 50% of the global population.

2. Materials and methods

2.1. Study sites

For this study, we selected four paddy rice flux sites, namely, the Mase paddy rice site in Japan, the Haenam paddy rice site in South Korea, the Twitchell Island paddy rice site in California, USA, and the Jingzhou paddy rice site in China (Table 1). For detailed descriptions of the four sites, see the AmeriFlux (http://ameriflux.lbl.gov/sites/siteinfo/US-Twt) and AsiaFlux (http://asiaflux.net/) websites, or the report by Su et al. (2013). The flux footprint of the four sites has been analyzed by Su et al. (2013) and Xin et al. (2017).

Table. 1
Characteristics of the four paddy rice CO_2 eddy flux sites.

Site name	Country	Lat (°)	Long (°)	Elevation (m)	Temp (°C)	Prec (mm)	Data availability	Rejection rates
Mase	Japan	36.05	140.03	13	13.5	1236	2003–2005	
Haenam	Korea	34.55	126.57	13.74	13.8	1306	2008	
Twitchell Island	USA	38.11	−121.65	−5	15.1	326	2011–2012	
		38.11	−121.65					
Jingzhou	China	30.34	112.12	32.2	16.5	1095	2010, 2013, 2018	50%, 56%, 32%

2.1.1. Mase paddy rice site, Japan

The Mase (MSE) paddy rice flux site (36.05°N, 140.03°E) is located in a rural area of Tsukuba city in central Japan, about 50 km northeast of Tokyo (Saito et al., 2005). The site is surrounded by artificially irrigated flat paddy rice fields measuring 1.5 km (north to south) by 1 km (east to west). The climate is warm and humid, with a mean annual air temperature of 13.5 °C and mean annual precipitation of 1236 mm. The paddy rice fields around the tower are planted with single-season rice, representing the regional cropping practice and calendar. The paddy rice fields are generally plowed, fertilized, and flooded in late April, transplanted in early May, begin to ear in late July and early August, and are harvested in mid/late September (Ono et al., 2015; Saito et al., 2007; Sasai et al., 2012).

2.1.2. Haenam paddy rice site, South Korea

The Haenam (HFK) paddy rice site (34.55°N, 126.57°E) is located in Haenam-gun, Jeollanamdo, South Korea (near the southwestern end of the Korean Peninsula), which is characterized by heterogeneous land cover types consisting of rice paddies and different patches of various land use (Kwon et al., 2010). The terrain around the flux tower is relatively flat, with an elevation of 13.7 m above sea level. The mean annual air temperature is 13.8 °C and the mean annual precipitation is 1306 mm (Ryu et al., 2008). The production model of this region is mainly two-crop rotation (other crops and paddy rice). The paddy rice fields are generally transplanted in early July and harvested in late September/-early October (Kwon et al., 2010).

2.1.3. Twitchell Island paddy rice site, USA

The Twitchell Island (TWT) paddy rice site (38.11°N, 121.63°W) is administered by the California Department of Water Resources, and is located on Twitchell Island in the Sacramento-San Joaquin Delta, California, USA, about 100 km inland from the Pacific Ocean (Knox et al., 2015). The region is dominated by a Mediterranean climate, with hot and dry summers and cool and wet winters. The mean annual air temperature is 15.1 °C and the mean annual precipitation is 326 mm. Two varieties of rice are planted from mid-April to May and harvested between late September and early November (Hatala et al., 2012; Knox et al., 2016, 2015).

2.1.4. Jingzhou paddy rice site, China

The Jingzhou (JZ) paddy rice site (30.34°N, 112.12°W) is administered by the agricultural meteorological experimental station in Jingzhou city, Hubei province, China. The site is located on the relatively flat Jianghan plain, which has a north subtropical monsoon climate. The annual mean air temperature is 16.5 °C and the annual mean precipitation is 1095 mm. Paddy rice is usually transplanted in early June and harvested in September (Su et al., 2013).

2.2. Eddy flux tower data

The availability/quality of measured NEE data is very important for model simulation, which may have a direct influence on GPP when NEE is subsequently divided into GPP and R_e (Reichstein et al., 2005). The availability of 30-min NEE data in the growing season of paddy rice at the four sites were statistically analyzed (Table 2), and the data processing procedure was briefly summarized.

2.2.1. MSE flux site

The CO_2 flux at the MSE flux site was measured by an open-path EC sensor. The equipment model, setting, calibration, and measurement of the flux tower have been described in previous studies (Saito et al., 2005). EC flux data contain a large number of errors due to instrument

Table. 2
The availability ratio of 30-min NEE for each 8-day period in the growing season of paddy rice in the four sites.

DOY	Mase			Haenam	Twitchell Island		Jingzhou		
	2003	2004	2005	2008	2011	2012	2010	2013	2018
137	0.71	0.47							
145	0.80	0.80	0.74						0.98
153	0.78	0.61	0.48		1.00		0.99	1.00	1.00
161	0.76	0.73	0.74	0.74	1.00		1.00	1.00	1.00
169	0.81	0.89	0.90	0.53	1.00		1.00	1.00	1.00
177	0.79	0.86	0.83	0.52	1.00	1.00	1.00	1.00	1.00
185	0.71	0.92	0.63	0.63	1.00	1.00	0.98	0.92	0.85
193	0.82	0.61	0.89	0.65	1.00	1.00	1.00	1.00	1.00
201	0.77	0.87	0.86	0.71	1.00	1.00	1.00	1.00	1.00
209	0.89	0.79	0.97	0.63	1.00	1.00	1.00	0.97	1.00
217	0.67	0.93	0.88	0.61	1.00	1.00	1.00	1.00	1.00
225	0.73	0.72	0.84	0.68	1.00	1.00	1.00	1.00	1.00
233	0.77	0.79	0.77	0.70	1.00	1.00	1.00	1.00	1.00
241	0.78	0.64	0.85	0.57	1.00	1.00	1.00	1.00	1.00
249	0.90	0.80	0.62	0.57	1.00	1.00	0.99	1.00	1.00
257	0.59	0.85	0.76	0.43	1.00	1.00			
265	0.53			0.71	1.00	1.00			
273				0.54	1.00	1.00			
281				0.70	1.00	1.00			
289						1.00			
297						1.00			
305						1.00			
313						1.00			

malfunction, atmospheric conditions inappropriate for EC measurements, rainfall, or human disturbances. To eliminate these errors, the EC data were subjected to quality control procedures, as described by Saito et al. (2005). The GPP and R_e were also estimated in the same way as Saito et al. (2005). Daily carbon flux data, PAR data, and air temperature data were averaged over an 8-day period, consistent with MODIS 8-day composites. Daily and 8-day data from 2003–2005 within the plant growing season were used in this study.

2.2.2. HFK flux site

The CO_2 flux at HFK was measured by an open-path EC sensor. Detailed information about the flux measurements, data processing, quality control, and gap-filling has previously been reported (Hong et al., 2009; Kwon et al., 2010). The data processing method, whereby NEE was separated into GPP and R_e, was the same as for the MSE flux site. The HFK site has no quantum sensor with which to directly measure the photosynthetic photon flux density (PPFD or PAR), so PAR was estimated to be 45% of the solar radiation (Meek et al., 1984) and the units of PAR were converted from W m^{-2} to μmol $m^{-2} s^{-1}$ (Aber et al., 1996; Dye, 2004). The daily GPP, NEE, and climate data in 2008 were averaged over an 8-day period according to the MODIS 8-day composite images. Daily and 8-day data from the paddy rice growing season in 2008 were used in this study.

2.2.3. TWT flux tower site

The CO_2 flux at TWT was measured by an open-path EC sensor. The half-hourly GPP data were downloaded from the AmeriFlux web site (http://ameriflux.ornl.gov/). The partitioning of NEE flux into GPP and R_e and the gap-filling of missing data were as described in previous studies (Baldocchi et al., 2015; Knox et al., 2016). Daily GPP, NEE, and climate data from 2011–2012 were averaged over an 8-day period (following the MODIS 8-day composites). Daily and 8-day data from the paddy rice growing season in 2011–2012 were used in this study.

2.2.4. JZ flux site

The flux densities of CO_2, water vapor, sensible heat, latent heat, and momentum, as well as the friction velocities over the paddy rice field, were measured by the EC method. Three-dimensional wind speeds and temperature fluctuations were measured with a sonic anemometer (CSAT3, Campbell Scientific, Inc., USA). An open-path infrared gas analyzer (LI-7500, LI-COR Inc., Lincoln, NE, USA) was used to measure the CO_2 flux and water vapor densities at the flux site. Both the CSAT3 and LI-7500 were installed at a height of 2 m above the ground with a sensor separation of 20 cm. The data from the sonic anemometer and analyzer were sampled at 10 Hz using a data logger (CR3000, Campbell Scientific, Inc., USA). The data logger is connected to the server through the direct communication method of network cable, and the data logger program can collect data online through the server. Raw data acquired at 10 Hz were processed using the post-processing software EddyPro, including spike removal, lag correction of H_2O/CO_2 relative to the vertical wind component, sonic virtual temperature correction, the performance of the planar fit coordinate rotation, corrections for density fluctuation (WPL correction), frequency response correction, etc. Similar to the test methods used in previous research (Alberto et al., 2009; Saito et al., 2005), we conducted a stationarity test and integral turbulence characteristics test (Aubinet et al., 2000; Foken and Wichura, 1996) to check the data. In addition to the above processing steps, the half-hourly flux data were screened according to the following criteria: (i) data were rejected when the sensor was malfunctioning (e.g., when there was a fault diagnostic signal), (ii) data were rejected when precipitation occurred within 1 h before and after the collection, (iii) incomplete 30-min data were rejected when the missing ratio was larger than 3% in the 30-min raw record, and (iv) data were rejected at night when the friction velocity was below 0.1 m s^{-1} (P. and Blanken 1998; Liu et al. 2011). The average annual rejection rates during the paddy rice growing season were 50% in 2010, 56% in 2013, and 32% in 2018. In the subsequent analysis, we only used the flux data that passed the above treatment.

2.2.5. Processing of the flux data

EC systems directly measure NEE rather than GPP. Thus, the NEE of CO_2 between the atmosphere and paddy rice fields was separated into GPP and R_e. To partition NEE into GPP and R_e, a conventional method that estimates the nighttime R_e (i.e., NEE in nighttime hours) as an exponential function of air temperature (T_a) was adopted. This function was applied to the daytime to estimate the daytime half-hourly R_e (Falge et al., 2001). The simple exponential function is:

$$R_e = A \times e^{(B \times Ta)} \tag{1}$$

where A and B are estimated model coefficients and T_a is the air temperature; B is related to a temperature coefficient, Q_{10}, as $B = \ln(Q_{10})/10$, and A denotes the value of R_e at 0 °C. Another commonly used method was employed to gap-fill the GPP values corresponding to the time points at which invalid NEE data had been removed (Falge et al., 2001). NEE is generally expressed as a rectangular hyperbolic function (the Michaelis–Menten light response equation) of incident PAR or incident PPFD (Q_P), which can be expressed as follows:

$$NEE = \frac{\alpha \times Q_P \times GEE_{max}}{\alpha \times Q_P + GEE_{max}} - R_e \tag{2}$$

where GEE_{max} (GPP at saturating light) and α (initial slope of the function or ecosystem quantum yield) are empirical constants that can be determined from a regression analysis of the NEE and incident PPFD. The daily NEE, R_e, and meteorological variables were estimated by summing the averaged half-hourly or hourly rate over 24 h. The GPP was estimated as the sum of the NEE and R_e. The relationship among GPP, NEE and R_e can be expressed as:

$$GPP = -NEE + R_e \tag{3}$$

The 8-day GPP mean value was calculated from the daily data. If more than two days of daily data within a given 8-day period were unavailable, the 8-day value was indicated as missing. In this study, the paddy rice growing period was divided into four phenological transitions, and the GPP of the respective transitions was estimated from the equations stated above.

2.3. MODIS data

The MODIS sensor on NASA's Terra satellite was launched in December 1999. Among the 36 spectral bands of MODIS, seven are mainly designed for studying vegetation and land surface: blue (459–479 nm), green (545–565 nm), red (620–670 nm), near-infrared (841–875 nm, 1230–1250 nm), and shortwave infrared (1628–1652 nm, 2105–2155 nm). The MODIS sensor has a spatial resolution of 250 m in the red and near-infrared bands, and 500 m in blue, green, and shortwave infrared bands. In our study, the 8-day land surface reflectance (MOD09A1, 500-m spatial resolution) datasets from NASA's Earthdata Search were employed.

Based on the geolocation information (latitude and longitude) of the paddy rice flux sites, the site-specific time series of land surface reflectance and quality flags in the study period were extracted from one MODIS pixel centered on the flux tower. Poor-quality observations were gap-filled using a three-step procedure (Jin et al., 2013). EVI and the land surface water index (LSWI) were calculated using 8-day synthesized surface reflectance data from four spectral bands (blue, red, near-infrared (841–875 nm), and shortwave infrared (1628–1652 nm)). EVI (Huete et al., 2002, 1997) and LSWI (Xiao et al., 2004a) were calculated as follows:

$$EVI = G \times \frac{\rho_{nir} - \rho_{red}}{\rho_{nir} + (C_1 \times \rho_{red} - C_2 \times \rho_{blue}) + L} \tag{4}$$

$$LSWI = \frac{\rho_{nir} - \rho_{swir}}{\rho_{nir} + \rho_{swir}} \tag{5}$$

2.4. Vegetation photosynthesis model

Based on the concept that a vegetation canopy is composed of chlorophyll (chl) and non-photosynthetic vegetation (NPV) that includes materials at both the canopy-level (e.g., stem, branch, senescent leaves) and leaf-level (e.g., cell walls, vein, and other pigments), VPM was developed to estimate the GPP over the photosynthetically active period of vegetation as the product of the PAR absorbed by chlorophyll ($APAR_{chl} = FPAR_{chl} \times PAR$) and LUE (Xiao et al., 2004a). Thus, VPM can be described as:

$$GPP = \varepsilon_g \times FPAR_{chl} \times PAR \tag{6}$$

where ε_g is the LUE for GPP (μmol CO_2/μmol PPFD) and PAR is in units of μmol PPFD. Within the photosynthetically active period of vegetation, $FPAR_{chl}$ is estimated as a linear function of EVI and a coefficient α; in this study, α is set to 1.0 (Xiao et al., 2004a, 2004b; Zhang et al., 2016):

$$FPAR_{chl} = \alpha \times EVI \tag{7}$$

The LUE value (ε_g) is affected by temperature and water, and can be expressed as:

$$\varepsilon_g = \varepsilon_0 \times T_{scalar} \times W_{scalar} \tag{8}$$

where ε_0 is the apparent quantum yield or maximum LUE (μmol CO_2/μmol PPFD, or g C/mol PPFD). In view of its variation with environmental conditions, ε_0 was estimated from four major phenological transitions of paddy rice instead of being assigned a constant value (see detailed description in Section 2.5). T_{scalar} and W_{scalar} are scalars for the effects of temperature and water on the LUE of vegetation, respectively. Using the equation developed for the terrestrial ecosystem model, the effect of temperature on photosynthesis (T_{scalar}) was estimated at each time step as:

$$T_{scalar} = \frac{(T - T_{min}) \times (T - T_{max})}{(T - T_{min}) \times (T - T_{max}) - (T - T_{opt})^2} \tag{9}$$

where T_{min}, T_{max}, T_{opt} denote the minimum, maximum, and optimal temperature for photosynthetic activity, respectively. In this study, T_{min} and T_{max} were set to 0 °C (cold damage to plants) and 48 °C (heat damage to plants), respectively, at all sites (Xin et al., 2017). T_{opt} was set to the average temperature in each of the four major phenological transitions (see detailed description in Section 2.5). If the air temperature fell below T_{min}, T_{scalar} was set to zero.

The effect of water on plant photosynthesis (W_{scalar}) was estimated from satellite-derived LSWI as:

$$W_{scalar} = \frac{1 + LSWI}{1 + LSWI_{max}} \tag{10}$$

where $LSWI_{max}$ is the maximum LSWI during the growing season of paddy rice for each pixel based on an analysis of seasonal LSWI dynamics derived from MODIS data. The maximum LSWI value within the paddy rice growing season was used as an approximation of $LSWI_{max}$.

2.5. Identification of phenological transitions of paddy rice

Paddy rice is grown in warm and waterlogged soil. The paddy fields are flooded throughout the growing season, providing ideal conditions for crops that release large amounts of CO_2. Four major phenological transitions (PTs) were derived from the annual MODIS EVI time series data: PT1, from the returning green stage after seedling establishment to tillering; PT2, from tillering to the panicle initiation stage; PT3, from the panicle initiation stage to heading; and finally PT4, from heading to harvest. Before the PTs were extracted, the EVI time series data from the four flux sites were chronologically combined and the quality of the EVI observations in each pixel was examined for contamination by cloud and snow. The very few poor-quality EVI observations were removed and the gaps were filled using a simple gap-filling method (Xiao et al., 2003). The Savitzky–Golay filter was then used to smooth the EVI observations so as to preserve peak moments among the data and reduce the biased low values caused by atmospheric effects (Chen et al., 2004; Savitzky and Golay, 1964). The two major parameters of this filter, namely the half-width of the smoothing window (m) and an integer specifying the degree of the smoothing polynomial (d), were empirically set to 4 and 2, respectively. Piecewise logistic functions were used to identify the PTs of paddy rice through inflection point estimates within the VI time series from the four flux sites (Zhang et al., 2003). The model can be expressed as follows:

$$y(t) = \frac{c}{1 + e^{a+bt}} + d \tag{11}$$

where time t is measured in days; $y(t)$ is the EVI value at time t; d is the initial background EVI value, which is generally the minimum EVI value in the time series; $c + d$ is the maximum EVI value; a and b are fitting parameters. The rate of change of the curvature of the fitted logistic model was used to identify the PT dates, as these often coincide with the time when the rate of change of the curvature of the logistic function achieves a local minimum or maximum (Zhang et al., 2003). The rate of change in curvature can be calculated as:

$$K' = b^3 cz \left\{ \frac{3z(1-z)(1+z)^3\left[2(1+z)^3 + b^2c^2z\right]}{\left[(1+z)^4 + (bcz)^2\right]^{\frac{5}{2}}} - \frac{(1+z)^2(1+2z-5z^2)}{\left[(1+z)^4 + (bcz)^2\right]^{\frac{3}{2}}} \right\} \tag{12}$$

where $z = e^{a+bt}$ and a, b, t are the same as in Eq. (11). We define the metrics Es, T, and HD as the dates at which the intersect of the fitting curve and the rate of change of the curvature of the fitting curve reach their first maximum, first minimum, and second maximum in the first half of the year. Similarly, the metrics He and Ha are defined as the dates at which the intersect of the fitting curve and the rate of change of the curvature of the logistic function achieve their first and second minima of the second half of the year. Thus, the length of the four major PTs can be calculated from the gaps between these metrics, with PT1 = Es − T, PT2 = HD − T, PT3 = He − HD, and PT4 = Ha − He.

2.6. Simulation of VPM

Based on the four major PTs of paddy rice, the maximum LUE was estimated using the Michaelis–Menten light response equation. The optimum temperatures were given by the 8-day mean temperatures of each PT. If the start date of each PT was located in the first half of one 8-day period, the 8-day mean temperature was used to estimate the optimum temperature in that PT. If the end date of each PT was located in the second half of one 8-day period, the 8-day mean temperature was used in the estimation of optimum temperature in that PT. Thus, the GPP was simulated in all four PTs based on the improved maximum LUE and optimum temperatures. This improved VPM is named phenology-based VPM (PVPM). Finally, the proposed PVPM was applied to the four paddy rice flux sites to estimate the GPP, with all other parameters the same as for conventional VPM.

The PTs derived from the MODIS EVI data at the four paddy rice flux sites were evaluated alongside other relevant research results. The GPP estimated from PVPM were compared with estimations from conventional VPM and MOD17A2H data as well as GPP derived from data at the flux sites. The determination coefficient (R^2) and root mean square error (RMSE) were calculated to assess the accuracy of each approach.

3. Results

3.1. Seasonal dynamics of climate, vegetation indices, and GPP_{EC}

Fig. 1 compares the air temperature and PAR across the four sites over several years. The seasonal dynamics of PAR at the four sites are similar, with comparatively high values in the summer. The seasonal dynamics of air temperature at the four sites are also similar, with the highest values observed in mid-summer.

A comparison of GPP_{EC} within the growing season among the four sites is shown in Fig. 2. At MSE, GPP_{EC} increases after the paddy rice is transplanted in early May, reaches its peak in late July/early August (>10 g C m^{-2} day^{-1}), and drops sharply by early September. At HFK, paddy rice GPP_{EC} starts to increase rapidly in mid-June, reaches its peak in mid-August (>10 g C m^{-2} day^{-1}), and declines quickly from mid-September into October. At TWT, GPP_{EC} starts to increase from late May to mid-June (about one month later in 2012), reaches its peak value of nearly 15 g C m^{-2} day^{-1} in August (September in 2012), and decreases until it is harvested in late October (mid-November in 2012). At JZ, the farmers transplant rice from late May to early June and harvest it in mid-September. GPP_{EC} starts to rise steadily in June, reaches its peak value in late July or early August, and gradually drops until it is harvested in mid-September. The 8-day maximum GPP_{EC} among these four sites (covering nine site-years) varies from 5–20 g C m^{-2} day^{-1} (Fig. 2).

Fig. 3 compares two VIs (EVI and LSWI) at the four sites. At MSE, EVI starts to gradually increase in May, and LSWI increases steeply in late April. Both VIs start to drop steeply in September. At HFK, EVI and LSWI increase steadily until mid-June and decrease quickly in September. At TWT, both EVI and LSWI rise gradually in June and start to decline in August (2011) or September (2012). At JZ, following the harvest of oilseed rape in late May, the field is flooded and rice plants are transplanted. EVI rises rapidly in mid-June, corresponding to the rapid rise in GPP_{EC} (Fig. 4). By early or mid-September, EVI and LSWI reach ~0.2 and ~0.1, respectively, corresponding to the harvest season of paddy rice.

3.2. Key PTs of paddy rice

The rates of change in the curvature of the fitted logistic models derived from flux tower EVI-based data are shown in Fig. 4. The EVI dynamics at the four flux sites are similar, with the highest value in mid-summer and the lowest value at the beginning of the growing season or after the harvest.

The day of the year (DOY) at the beginning and at the end of the four PTs are summarized in Table 3. The length of the plant growing season (LOS) is somewhat different at the four sites. At MSE, the LOS varies from 109–125 days, with an average LOS of 117 days from 2003–2005. At HFK, the LOS is 115 in 2008, almost the same as the average LOS at MSE. The LOS at TWT is greater than 135 days in both 2011 and 2012. At JZ, the LOS is less than 100 days in 2010, 2013, and 2018, and the variations among the LOS are very small. In terms of the start date of PT1 (SDPT), MSE has a similar date in 2003 and 2004 (DOYs of 142 and 143), whereas the SDPT in 2005 is about one week later. The SDPT at HFK is 168, later than that of MSE. At TWT, the SDPT in 2012 is nearly one month later than that in 2011. At JZ, the SDPT is similar in 2010, 2013, and 2018 (DOYs of 158,155, and 152, respectively). At MSE, TWT, and JZ, the SDPT is relatively close (except TWT in 2012). With regard to the end date of PT4 (EDPT), MSE and JZ exhibit small variations, whereas HFK and TWT are similar in 2011 (Table 3).

To validate the PTs of paddy rice across the four sites, as much information as possible was collected from the literature. At MSE in 2003 and 2004, rice seedlings were transplanted in early May and harvested in mid-September (Inoue et al., 2008; Lee et al., 2017). Usually, rice seedlings will turn (or return) green ~7–35 days (depending on rice variety, meteorology of site location, and local environmental factors) after planting or transplanting (Saichuk et al., 2009). From this perspective, an SDPT in late May and an EDPT in mid-September are reasonable. According to previous research, rice planting and harvesting

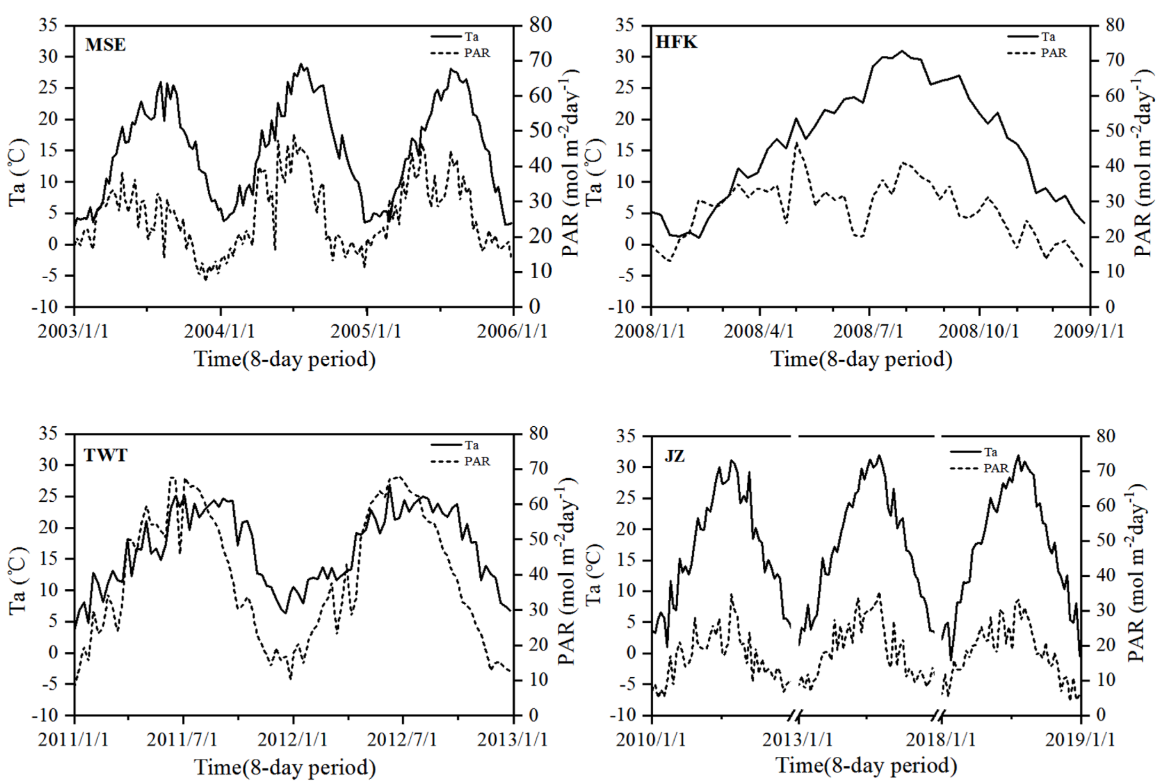

Fig. 1. Seasonal dynamics of PAR and air temperature (T_a) from flux measurements at the four CO_2 eddy flux sites. (a) MSE, Japan, 2003–2005; (b) HFK, South Korea, 2008; (c) TWT, California, USA, 2011–2012; (d) JZ, China, 2010, 2013, and 2018.

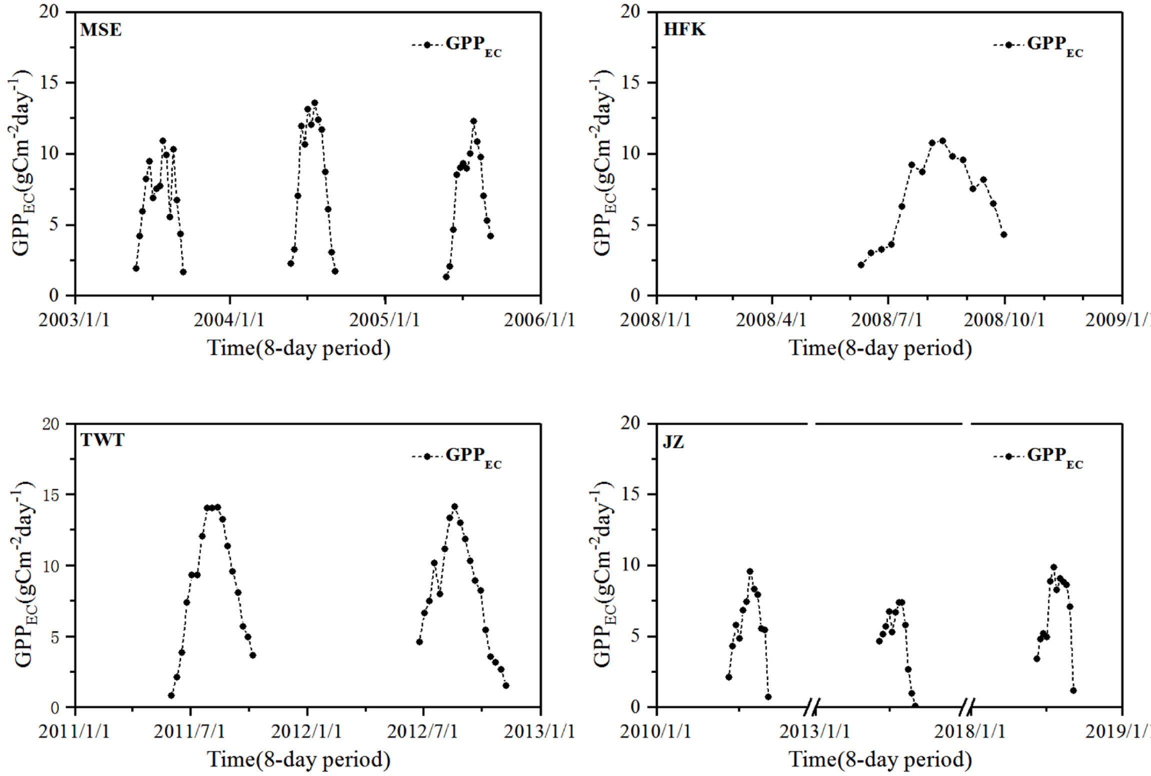

Fig. 2. Temporal dynamics of GPP (GPP$_{EC}$) estimated from flux measurements at the four CO_2 eddy flux sites within growing seasons. (a) MSE, 2003–2005; (b) HFK, 2008; (c) TWT, 2011–2012; (d) JZ, 2010, 2013, 2018.

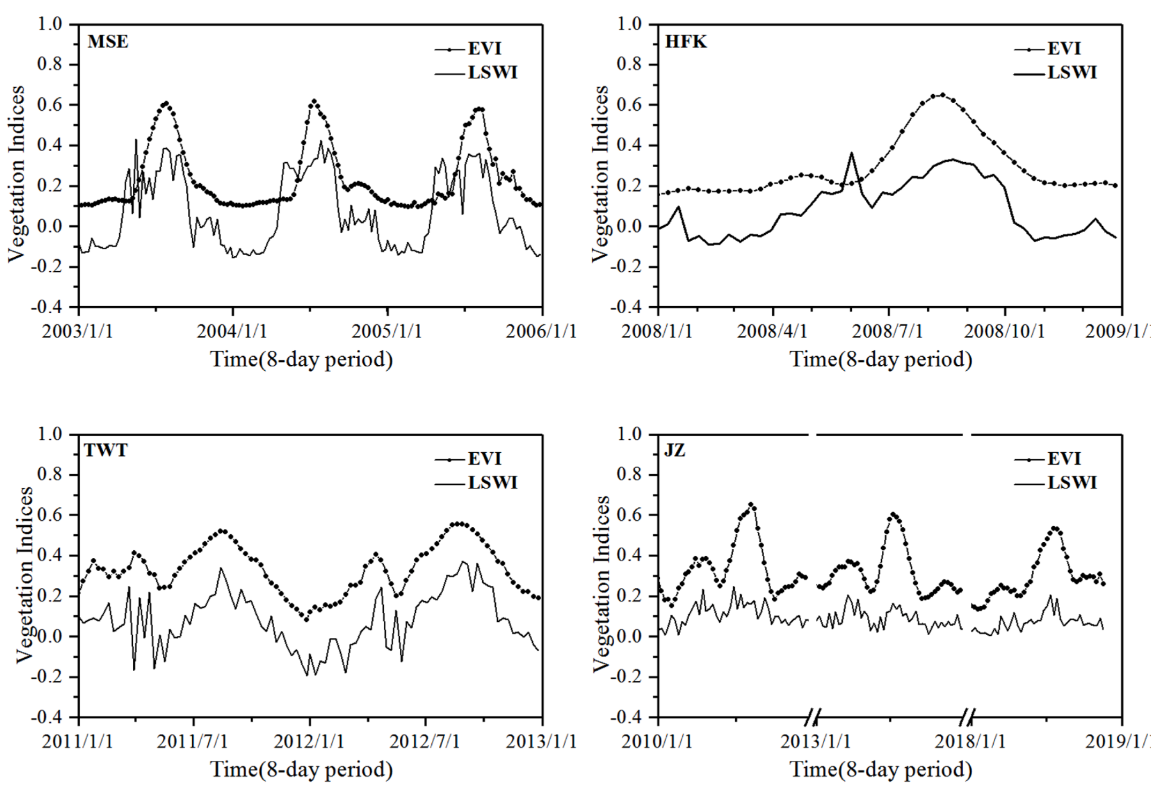

Fig. 3. Seasonal dynamics of two MODIS-derived VIs (EVI and LSWI) at the four CO_2 eddy flux sites. (a) MSE, 2003–2005; (b) HFK, 2008; (c) TWT, 2011–2012; (d) JZ, 2010, 2013, 2018.

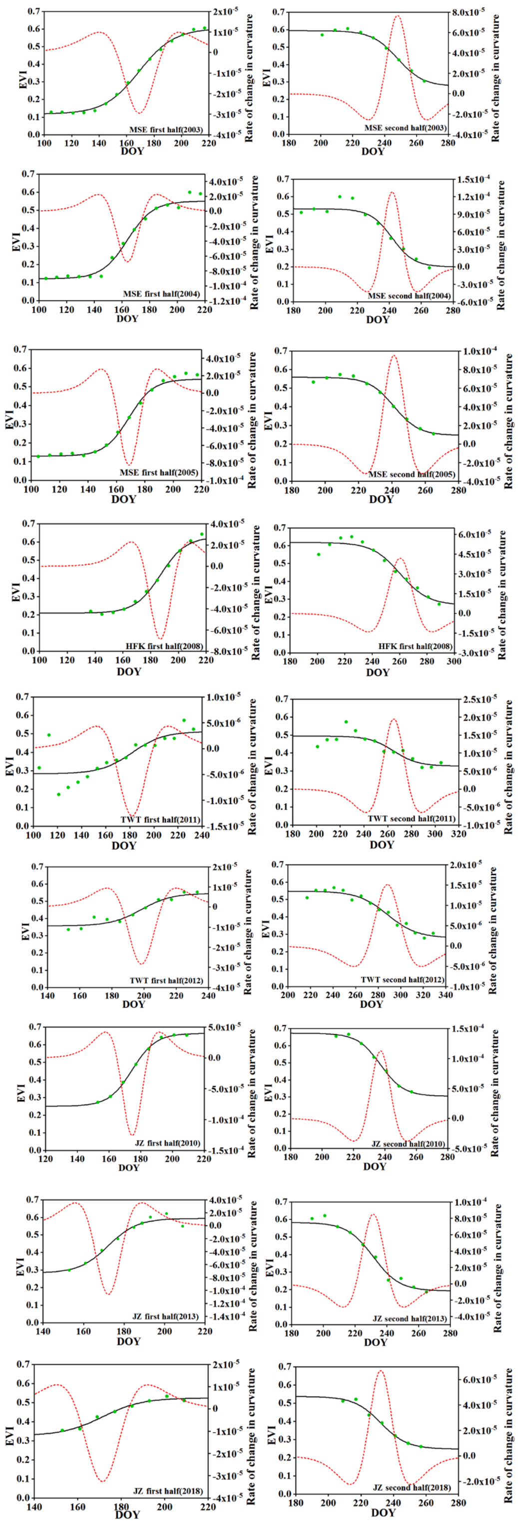

Fig. 4. Rate of change in curvature (red dot lines) of the fitted logistic models derived from EVI-based data over flux sites (green dots are 8-day EVI, black solid lines are fitted logistic models).

occurred in early June and early October at HFK in 2008 (Kwon et al., 2010). The SDPT in mid-June and the EDPT in early October are in good agreement with this research. At TWT, the general schedule calls for planting in mid/late April and harvesting between late September and late October, with the exception of 2012, when planting was delayed until mid-May due to a late rainy season (Knox et al., 2016). The planting time lag in 2012 and the SDPT in early June were detected in our research. Previous studies at JZ show that the transplanting date is usually in early June and the turning-green date lags by around one week, with the harvest time typically in early/mid-September (Su et al., 2013). This agrees well with our SDPT in early June and harvest date in mid-September.

3.3. Estimation of maximum LUE (ε_0) and optimum temperature during PTs

Based on the four PTs extracted from the MODIS EVI data, the maximum LUE and optimum temperature were estimated using the CO_2 flux data and climate data from the four flux sites. In a previous study of GPP estimations for paddy rice, the maximum LUE (ε_0) was set to 0.05 mol CO_2/mol PPFD (0.6 g C/mol PPFD) (Xin et al., 2017). However, this quantity varies considerably during the four PTs over the four flux sites (Table 4). At MSE from 2003–2005, the maximum ε_0 appears in PT2 and varies from 0.058–0.065, while the minimum appears in PT1 or PT4 and varies from 0 to 04. At HFK, the maximum ε_0 is 0.047 in PT4, while the minimum ε_0 is 0.036 in PT1. At TWT in 2011 and 2012, the maximum ε_0 changes from 0.038 to 0.04 and appears in PT3, while the minimum ε_0 is 0.02 in PT1. At JZ in 2010, the maximum ε_0 is 0.05 in PT2 and the minimum ε_0 is 0.03 in PT3 and PT4. For the other years at this site (2013 and 2018), the maximum ε_0 is 0.045 in PT4 and the minimum ε_0 is 0.03 in PT2 (2013) and PT1 (2018).

In a previous study on GPP estimations for paddy rice, the relationship between the daily mean air temperature and the GPP from flux data was investigated as a means of defining the optimum temperature (T_{opt}) (Xin et al., 2017). Table 5 presents the improved optimum temperatures estimated from the PTs at the four flux sites (T_{popt}). At MSE from 2003–2005, T_{popt} varies from 19.31–27.06 °C. At HFK, the maximum T_{popt} is 27.98 °C in PT3, while the minimum T_{popt} is 23.24 °C in PT1. At TWT, T_{popt} ranges from 16.66–20.83 °C. The maximum T_{popt} occurs in PT2 of 2011, whereas the minimum occurs in PT4 of 2012. At JZ, T_{popt} varies from 25.28–30.51 °C. Over the three years considered in this study, the maximum T_{popt} values occur in PT3, whereas the minimum values occur in PT1. Generally, there are substantial differences between the optimum temperatures in each PT (T_{popt}) and the optimum temperature over the growing season (T_{opt}) at all four flux sites.

3.4. Temporal dynamics of GPP as predicted by PVPM within growing seasons

The temporal dynamics of GPP predicted by PVPM (GPP_{PVPM}) are plotted against the temporal dynamics of GPP_{EC} derived from the individual flux sites (nine site-years) in Fig. 5. At MSE, GPP_{PVPM} accurately tracks both the seasonal dynamics and inter-annual variation of GPP_{EC} from 2003–2005, except for some slight overestimation of the GPP_{EC} peak period in 2005. At HFK, GPP_{PVPM} rises sharply in July, reaches a peak in August, and drops rapidly in late September, which clearly tracks the temporal dynamics of GPP_{EC}. At TWT, GPP_{PVPM} agrees well with GPP_{EC} in 2011 in terms of the seasonal maximum. The 8-day maximum GPP_{PVPM} value is slightly higher than GPP_{EC} in 2012 (Fig. 5). At JZ, GPP_{PVPM} tracks both the seasonal dynamics and inter-annual variation of GPP_{EC} well in 2010, 2013, and 2018. There are some slight differences at the heading stage of paddy rice in 2018. Overall, the temporal dynamics of GPP_{PVPM} and GPP_{EC} are in good agreement at all four sites.

Scatterplots of GPP_{PVPM} and GPP_{EC} over the paddy rice growing seasons exhibit strong linear correlations at all four paddy rice sites (Fig. 6). The correlation between GPP_{PVPM} and GPP_{EC} was also compared with that between GPP_{VPM} and GPP_{EC} based on the same temporal data (see detailed discussion in Section 4.2). The coefficient of determination is greater than 0.9 at all four flux sites. HFK has the highest R^2 of 0.95, while TWT has the largest RMSE of 1.22 g C m^{-2} day^{-1}.

Table. 3
DOY of the PTs of paddy rice at the four CO_2 flux sites (PT1: from turning green stage after seedling establishment to tillering; PT2: from tillering to panicle initiation stage; PT3: from panicle initiation stage to heading; PT4: from heading to harvest).

Site name	Data availability	PT1(DOY)	PT2(DOY)	PT3(DOY)	PT4(DOY)	LOS
Mase	2003	142–168	169–195	196–230	231–266	125
	2004	143–165	166–186	187–227	228–258	116
	2005	150–169	170–188	189–225	226–258	109
Haenam	2008	168–188	189–208	209–239	240–282	115
Twitchell Island	2011	153–181	182–210	211–242	243–288	136
	2012	178–198	199–220	221–260	261–315	138
Jingzhou	2010	158–174	175–191	192–220	221–253	96
	2013	155–172	173–188	189–213	214–250	96
	2018	152–171	172–190	191–214	215–251	100

Table. 4
Comparison of maximum LUE used in PVPM and VPM.

Site Name	Year	VPM-based ε_0 (mol CO2/mol PPFD)	PVPM-based ε_0 (mol CO2/mol PPFD)			
			PT1	PT2	PT3	PT4
Mase	2003	0.05	0.035	0.060	0.051	0.049
	2004		0.030	0.058	0.045	0.030
	2005		0.047	0.065	0.047	0.040
Haenam	2008		0.036	0.040	0.038	0.047
Twitchell Island	2011		0.020	0.037	0.038	0.035
	2012		0.020	0.030	0.040	0.025
Jingzhou	2010		0.032	0.050	0.030	0.030
	2013		0.038	0.030	0.033	0.045
	2018		0.030	0.033	0.035	0.045

Table. 5
Comparison of optimum temperature between PVPM and VPM.

Site Name	Year	T_{opt} (°C)	T_{popt} (°C)			
			PT1	PT2	PT3	PT4
Mase	2003	20.00	19.31	21.07	22.53	24.56
	2004		21.61	23.29	27.06	24.75
	2005		19.65	24.35	25.61	26.46
Haenam	2008	25.00	23.24	27.47	27.98	24.55
Twitchell Island	2011	18.00	18.44	20.83	20.31	19.26
	2012		20.36	20.72	20.77	16.66
Jingzhou	2010		25.28	28.69	29.33	26.25
	2013		25.91	29.18	30.51	28.61
	2018		26.28	27.46	30.47	29.74

4. Discussion

4.1. Performance of GPP_{EC} and daily air temperature, VIs in four PTs of paddy rice fields

The relationship between GPP_{EC} and daily mean air temperature (T_a) through the entire growing season has been described in previous research on paddy rice GPP estimation (Alberto et al., 2009; Saito et al., 2005; Xin et al., 2017). Generally, GPP_{EC} increases with T_a until it becomes saturated at a certain temperature. As PVPM is based on the phenology of paddy rice, the relationship between GPP_{EC} and T_a during the PTs is investigated through the correlation between these parameters in PT1, PT2, PT3, and PT4. The results are shown in Fig. 7. In PT1, GPP_{EC} gradually increases as temperature rises, except at TWT in 2012, where GPP_{EC} first decreases with increasing temperature before increasing as the temperature rises further. At MSE, HFK, and JZ, the variation in GPP_{EC} ranges from 0–5 g C m^{-2} day^{-1} during PT1. The variation in GPP_{EC} at TWT has a broader range of 0–10 g C m^{-2} day^{-1}. At MSE in PT2 and PT3, GPP_{EC} rises as T_a increases, and appears to saturate (or plateau) at ~25 °C. This behavior is different from that reported in previous studies, which suggested a plateau at ~20 °C (Xin et al., 2017). At JZ in PT2 and PT3, GPP_{EC} increases as T_a rises, plateauing at ~29 °C. At HFK in PT2, GPP_{EC} climbs as T_a increases, and reaches a peak at ~29 °C. However, there is no significant trend in PT3 at this site. This may be because only a single year of flux data was used in this research. At TWT in PT2 and PT3, GPP_{EC} first increases as the temperature rises, before reaching a peak and decreasing as T_a increases further. In PT4, the relationship between GPP_{EC} and T_a is broadly consistent at all four flux sites, with GPP_{EC} increasing as T_a rises.

Fig. 8 illustrates the relationship between the 8-day EVI and the corresponding GPP_{EC} in the four PTs across three sites (HFK is neglected in this analysis because the 8-day GPP_{EC} and EVI data only covered a single year). Simple quadratic polynomial regression analyses show that GPP_{EC} is strongly correlated with EVI during all four PTs at TWT. This conclusion is slightly inconsistent with previous results, which indicated a strong linear relationships between GPP_{EC} and EVI over the full growing seasons at TWT (Xin et al., 2017). One potential reason for the lack of a linear correlation in the present study is that data from two years (2011 and 2012) were used in this research, whereas Xin et al. (2017) used data from a six-year period (2009–2014). At MSE and JZ, GPP_{EC} exhibits a strong relationship with EVI in PT1 and PT4. However, the relationship becomes weaker in PT3 at MSE. These results indicate that GPP_{EC} rises as EVI increases in the early growing season, and declines as EVI decreases at the end of the growth period. In the peak growing season (especially in PT3), EVI remains in a relatively narrow range with small variations, which is consistent with the idea that EVI should be in a stable range with high values during the heading period of paddy rice.

4.2. Comparison among GPP_{EC}, $GPPP_{VPM}$, GPP_{VPM}, and GPP from the MOD17A2H data product

The estimation of GPP from PVPM is more accurate than the GPP determined from directly flux the sites (Fig. 5). Additionally, comparisons of GPP_{PVPM} vs. GPP_{EC} and GPP_{VPM} vs. GPP_{EC} at the same site and within the same year are shown in Fig. 6. Based on fixed values of ε_0 and the optimum temperature, the VPM used in Xin's study was employed to simulate the GPP of rice paddy plants at sites in Japan, South Korea, and the USA. At JZ, fixed parameters were set to estimate GPP_{VPM} (Xin et al., 2017). At all four sites, the correlation between GPP_{PVPM} and GPP_{EC} is stronger than that between GPP_{VPM} and GPP_{EC}, and the RMSE of GPP_{PVPM} vs. GPP_{EC} is lower than that of GPP_{VPM} vs. GPP_{EC}.

MOD17A2H is a widely used global GPP data product, and has been applied in many studies of forests, grasslands, and crops (Fu et al., 2017; Tagesson et al., 2017; Wang et al., 2017). Recently, it has been suggested that GPP from the MOD17A2H product underestimates GPP_{EC} (Gitelson et al., 2014; He et al., 2014; Zhang et al., 2017). Fig. 9 compares GPP_{EC}, GPP_{VPM}, GPP_{PVPM}, and $GPP_{MOD17A2H}$ at the four paddy rice sites. $GPP_{MOD17A2H}$ is significantly lower than GPP_{EC}, GPP_{VPM}, and GPP_{PVPM} at all four sites during the crop growing season. Thus, the simulation accuracy of VPM is greater than that of $GPP_{MOD17A2H}$. However, GPP_{VPM} is slightly higher than GPP_{EC} at MSE in 2004 during the peak growing season. Furthermore, it yields moderate overestimates at HFK in the first half of the growing season in 2008, and produces similar overestimates

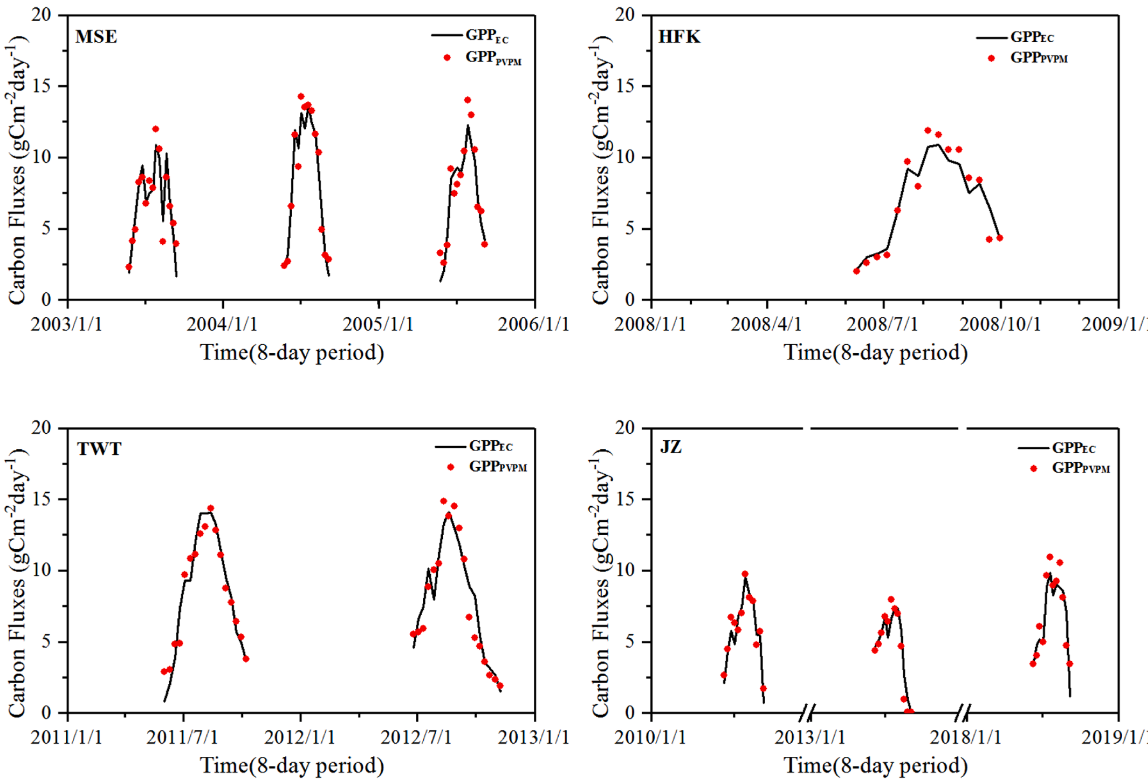

Fig. 5. Temporal dynamics of predicted and estimated GPP (GPP_{PVPM} and GPP_{EC}) at the four CO_2 eddy flux sites. (a) MSE, 2003–2005; (b) HFK, 2008; (c) TWT, 2011–2012;(d) JZ, 2010, 2013, and 2018.

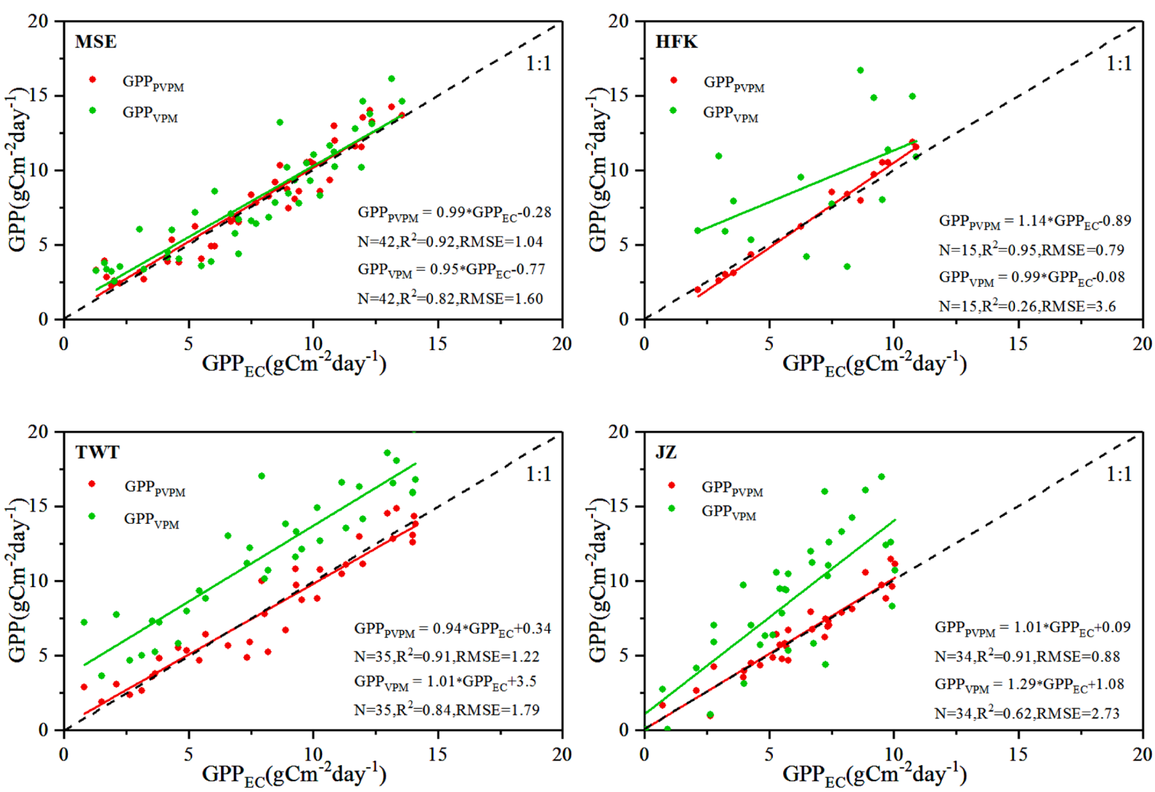

Fig. 6. Comparison of measured GPP and predicted GPP (GPP_{VPM}, GPP_{PVPM}, and GPP_{EC}) during growing seasons at the four rice paddy CO_2 eddy flux sites. (a) MSE, 2003–2005; (b) HFK, 2008; (c) TWT, 2011–2012; (d) JZ, 2010, 2013, 2018.

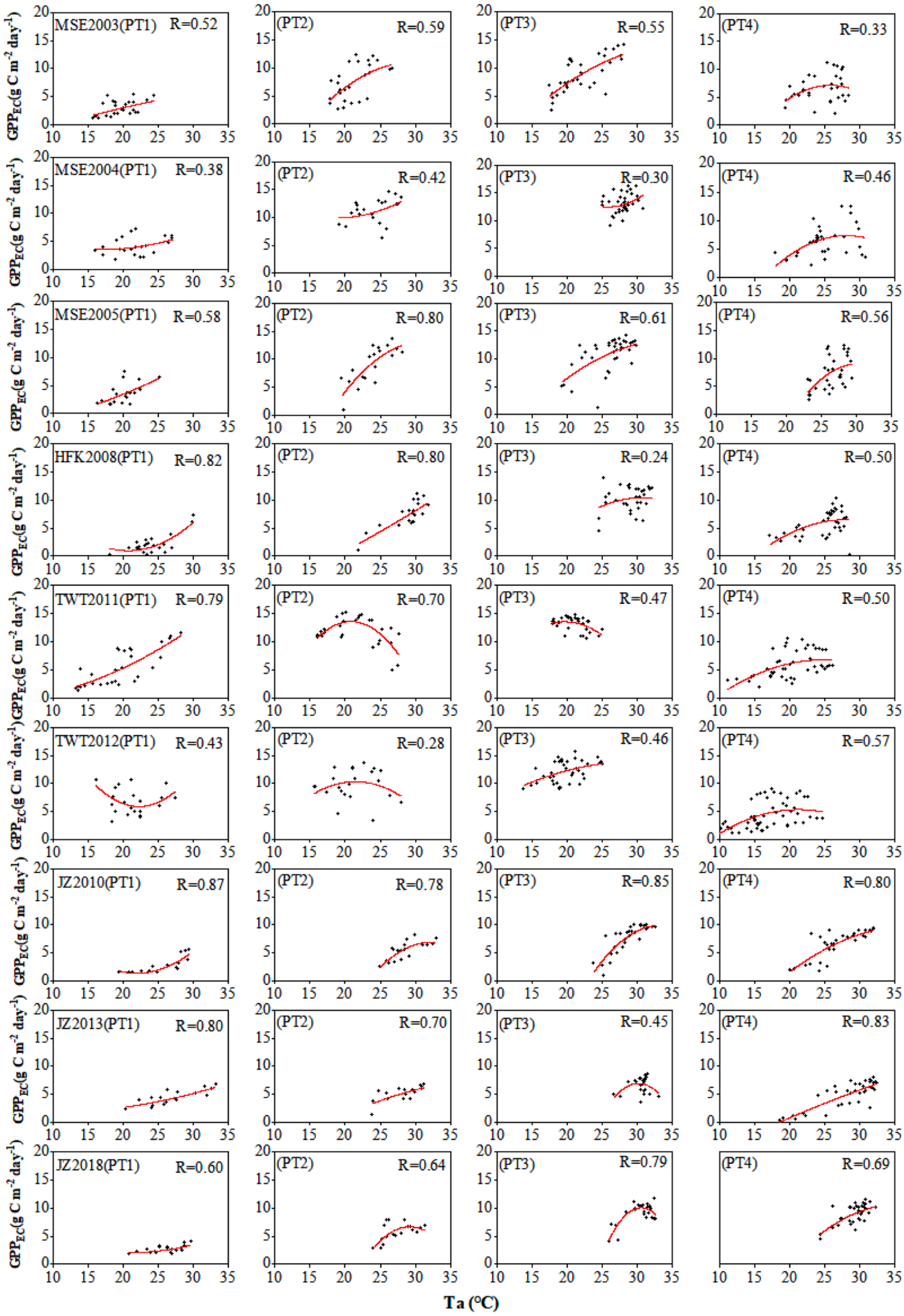

Fig. 7. Relationships between GPP$_{EC}$ and T$_a$ during the four PTs at the four flux sites. (a) MSE, 2003–2005; (b) HFK, 2008; (c) TWT, 2011–2012;(d) JZ, 2010, 2013, 2018.

in the peak of the growing season at TWT in 2011–2012 and at JZ in 2010, 2013, and 2018. The substantial underestimation in GPP$_{MOD17A2H}$, relative to GPP$_{EC}$, GPP$_{VPM}$, and GPP$_{PVPM}$, can be attributed to the climate data and the maximum LUE parameter used by Xin et al. (2017). The moderate overestimation in GPP$_{VPM}$, relative to GPP$_{EC}$ and GPP$_{PVPM}$, may be the result of the value of ε_0 used in the model. The maximum LUE is an essential parameter in LUE models, but suffers from significant uncertainty among different models and biome types. In the MOD17A2H data product, the moderate resolution imaging spectroradiometer photosynthesis (MODIS-PSN) model uses 0.22 g C/mol PPFD (1.004 g C/MJ) as its ε_0 parameter for croplands (see the Daily GPP and Annual NPP (MOD17A2/A3) Products NASA Earth Observing System MODIS Land Algorithm). In a previous GPP estimation study, ε_0 was set to 0.6 g C/mol PPFD (0.05 mol CO_2/mol PPFD) for VPM simulations of paddy rice (Xin et al., 2017). Compared with the ε_0 value used in the MOD17A2H data product and the VPM estimation of paddy rice, the value of ε_0 estimated from the four PTs in PVPM may be more appropriate, as this allows GPP$_{PVPM}$ to capture seasonal variations in GPP$_{EC}$ among the four paddy rice sites.

4.3. Comparison between GPP$_{EC}$, GPP$_{PVPM}$, GPP$_{PVPM_LUE}$, and GPP$_{PVPM_Topt}$

The optimum temperature (T$_{opt}$) is another key parameter in the LUE

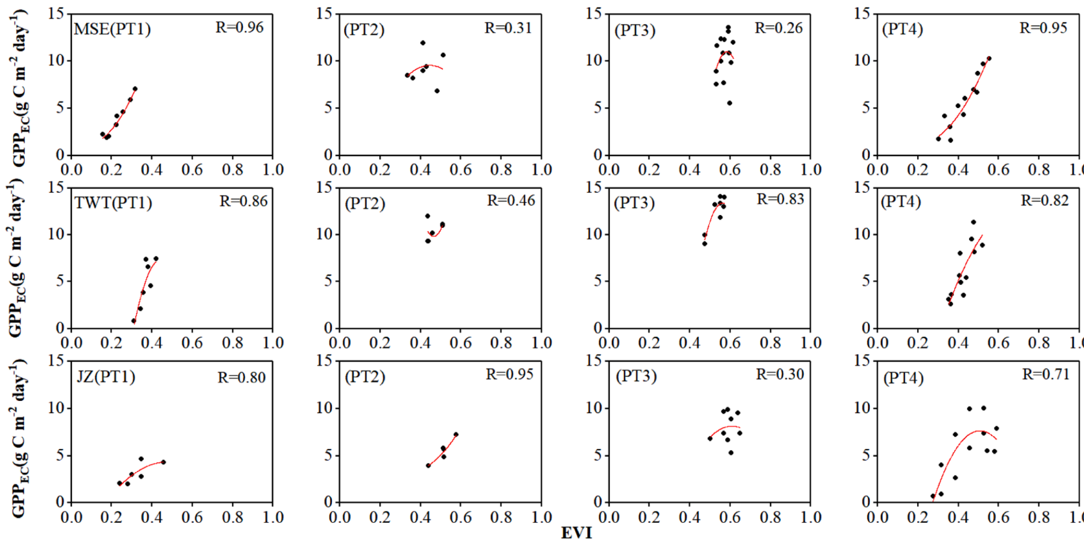

Fig. 8. Relationships between 8-day EVI and GPP_{EC} during the four PTs of the crop growing season. The top, middle, and bottom panels show the relationships at MSE (2003–2005), TWT (2011–2012), and JZ (2010, 2013, 2018), respectively.

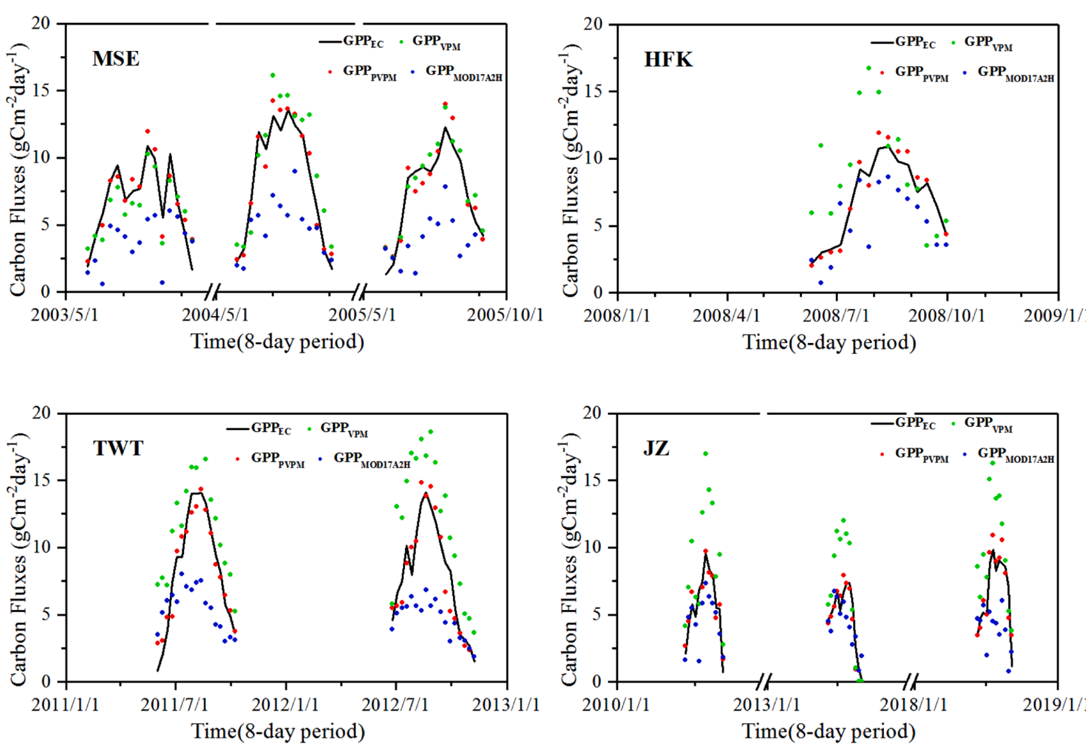

Fig. 9. Comparison of predicted and measured GPP (GPP_{VPM}, GPP_{PVPM}, $GPP_{MOD17A2H}$, and GPP_{EC}) during growing seasons at the four CO_2 eddy flux sites. (a)MSE, 2003–2005; (b)HFK, 2008; (c)TWT, 2011–2012;(d) JZ,2010, 2013, 2018.

model that often varies among models and biome types. A review paper highlighted the temperature acclimation and adaptation of photosynthesis for C_3 and C_4 plants (Yamori et al., 2014). Recently, a study on NPP revealed that, for forest GPP estimation from the CASA model, the optimum temperature defined in the peak of the growing season was more appropriate than that determined by the mean temperature of the month in which NDVI reaches its maximum (Pei et al., 2018). From this viewpoint, T_{popt} was averaged over the four PTs defined in this study. Xin et al. (2017) used values of 20 °C, 25 °C, and 18 °C as their T_{opt} parameters for paddy rice in VPM. To evaluate the performance of the improved optimum temperature and maximum LUE, the GPP values estimated from the improved T_{opt} (GPP_{PVPM_Tpopt}), from the improved maximum LUE (GPP_{PVPM_LUE}), and from combining the improved T_{opt} and maximum LUE (GPP_{PVPM}) were compared with GPP_{EC}. Fig. 10 shows the results. There is a substantial overestimation in GPP_{PVPM_Tpopt} compared with GPP_{PVPM} and GPP_{EC} during the peak growing season at HFK, TWT, and JZ. This demonstrates the degree of uncertainty in GPP estimates of paddy rice when using only the 8-day mean temperature as the optimum temperature in the PTs. Nevertheless, using PTs to estimate the optimum temperature is reasonable, and satellite-based VIs make it possible to delineate accurate PTs (Wang and Wu, 2019; Wu et al., 2017; Yamori et al., 2014). Additional research should compare the T_{popt} values derived from various methods. GPP_{PVPM_LUE} is slightly lower than GPP_{EC} at TWT in 2012 and slightly higher than GPP_{EC} in the peak

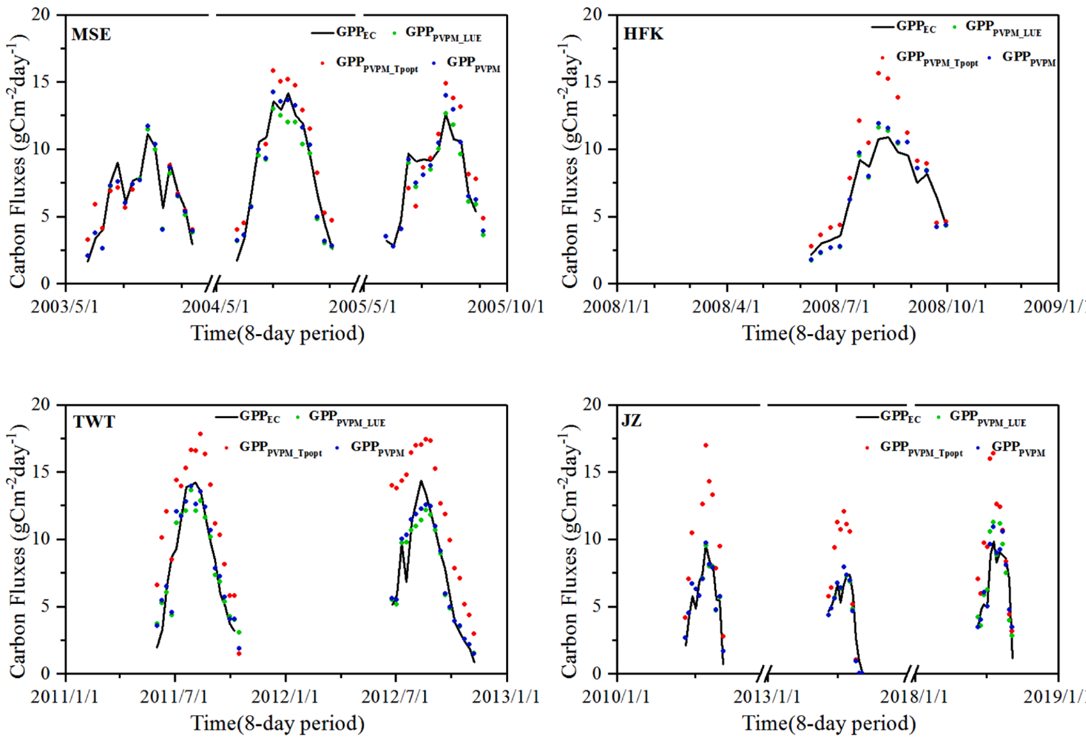

Fig. 10. Comparison of GPP_{PVPM_Tpopt}, GPP_{PVPM_LUC}, GPP_{PVPM}, and GPP_{EC} during growing seasons at the four CO_2 eddy flux sites. (a)MSE, 2003–2005; (b)HFK, 2008; (c)TWT, 2011–2012;(d) JZ,2010, 2013, 2018. GPP_{PVPM_Tpopt} – the GPP values estimated from the improved Topt; GPP_{PVPM_LUC} – the GPP values estimated from the improved maximum LUE.

growing season at HFK and JZ in 2018. A comparison of GPP_{PVPM_LUE} and GPP_{EC} implies that the maximum LUE estimation in the PTs is helpful in approaching the observed GPP. Generally, with regard to the improved maximum LUE and optimum temperature, GPP_{PVPM} tracks GPP_{EC} more accurately than GPP_{PVPM_LUE} and GPP_{PVPM_Tpopt} at the four paddy rice sites. This comparison suggests that both the maximum LUE and T_{popt} estimated using the PTs of paddy rice could be of great value for GPP estimation.

4.4. Sources of error and uncertainty in GPP estimation from PVPM in paddy rice cropland

The results of this research demonstrate that the temporal dynamics of GPP_{PVPM} agree well with those of GPP_{EC} (Figs. 5 and 6), with some acceptable overestimation in the peak of the growing season at MSE (in 2005) and JZ (in 2018). PTs were introduced into the GPP estimation of paddy rice. Many methods of deriving land surface phenology indicators from remotely sensed data or CO_2 EC measurements have been developed, but there is no wholly appropriate method for extracting temporal information on paddy rice. Recently, a rule-based algorithm called PhenoRice was developed for the automatic extraction of phenology information on rice crops (Boschetti et al., 2017). Because the test sites used to develop PhenoRice (Italy, India, and Philippines) are totally different from the sites considered in this study, there could be many uncertainties in terms of diverse genetics, environmental conditions, and management techniques. Thus, a traditional and comprehensive method of deriving vegetation phenology (Zhang et al., 2003) was employed, and the good agreement between the PTs of paddy rice and phenology information derived from the literature demonstrates the rationality of the method applied in this study. As the benefits and limitations of the method have already been discussed (Verbesselt et al., 2010; White et al., 2014; Zhang et al., 2004), additional work should focus on using more paddy rice flux sites and data from additional years to provide a more comprehensive comparison of different phenology extraction methods.

Maximum LUE is one of the main parameters in the PVPM. Two previous in-situ studies estimated the maximum LUE in predicting rice yields in the Philippines, Italy, and the USA, and found that this parameter varied in the range 0.08–0.20 mol CO_2/mol PPFD (Campbell et al., 2001; Kiniry et al., 2001). In another case of rice GPP estimation, the maximum LUE was set to ~0.1 mol CO_2/mol PPFD in the derivation of an LUE model (Chen et al., 2011). In a recent study of GPP estimation in paddy rice fields, 0.05 mol CO_2/mol PPFD was applied at four sites in Asia and the USA (Xin et al., 2017). Table 4 demonstrates that there is some discrepancy between the maximum LUE over a complete growing season and during the PTs, which is consistent with expert knowledge that the maximum LUE varies among the same ecosystem type over different regions (Xiao et al., 2011; Xue et al., 2016). The good agreement between GPP_{PVPM} and GPP_{EC} in our study implies that the maximum LUE estimated in the PTs reduces the uncertainty of this parameter and provides a substantial improvement in GPP estimations for paddy rice cropland. Another potential source of error is the uncertainty of climate datasets such as PAR (Cai et al., 2014; Cheng et al., 2014; He et al., 2014) and temperature. Remotely sensed data are rarely used in studies on the optimum temperature of paddy rice in GPP estimation. Although the improved optimum temperature has a limited impact in our study, the trends in optimum temperature in the PTs of paddy rice crops conform to the rhythms of rice growth, and could be used to promote growth in future research. The third main potential source of error concerns the estimation of site-based GPP_{EC}. In this study, different methods were used to calculate GPP_{EC} at four sites, which may have introduced extra uncertainty into the comparison between GPP_{PVPM} and GPP_{EC}. Other sources of error, such as the uncertainty of EVI time series data derived from MODIS imagery and mismatches in the spatial relationship between the footprint of a CO_2 flux tower and a MODIS pixel, were discussed by Xin et al. (2017).

5. Conclusions

The integration of PTs derived from time series of MODIS images and CO_2 flux measurements from eddy flux sites at four paddy rice sites has been used to obtain accurate GPP estimations. The GPP_{EC} data from the flux sites exhibit various trends with respect to daily mean air temperature during the PTs, rather than the single trends generalized from the entire growing season. The observed CO_2 flux data also present diverse tendencies with respect to the EVI time seris from MODIS during the PTs, in contrast to the single trends inferred from the full growing season. For this reason, the estimation of driving parameters in LUE models according to the land surface phenology is an effective way of improving GPP estimation.

Taking into account the uncertainty of the maximum LUE and optimum temperature in VPM, these parameters were estimated from the four major PTs corresponding to the physiological features of paddy rice. This is the first case study to use a phenology-based strategy to optimize the maximum LUE and optimum temperature in the GPP estimation of paddy rice croplands. The results indicate that estimating the maximum LUE and optimum temperature in PTs is more appropriate, in terms of capturing the temporal dynamics and inter-annual variations of GPP at paddy rice sites, than attempting to improve either the maximum LUE or optimum temperature. To complement and improve the global flux network, further assessment of the phenology-based LUE model at other paddy rice sites with comparative CO_2 flux measurements would be of great value in determining universal parameter values across various regions. The extrapolation of site-scale flux measurements to the regional or national scale should be achievable in the near future using the presented methodology.

6. Funding

This work was supported by the Strategic Priority Research Program A of the Chinese Academy of Sciences [grant number XDA23100201], East China University of Technology Ph.D. Project, China under Grant [grant number DLLJ20190179] and Key Laboratory for Digital Land and Resources of Jiangxi Province, East China University of Technology, China under Grant [grant number DHBK202005], Science & Technology Basic Resources Investigation Program of China under Grant [grant number 2017FY100901], the National Science Foundation of China under Grant [grant numbers 31,971,491, 41,701,449], the project of Ministry of Ecology and Environment under Grant [grant number 2019HJ2096001006], Key Laboratory of Aquatic Botany and Watershed Ecology, Chinese Academy of Sciences under Grant [grant number Y852691s01], Science and Technology Development Fund Research and project of Hubei Meteorological Bureau [grant number 2019Z04]

Declaration of Competing Interest

The authors declare that they have no known competing financial interests or personal relationships that could have appeared to influence the work reported in this paper.

Acknowledgements

We are grateful to the Earth Observation and Modeling Facility (EOMF) from the University of Oklahoma for providing technical support of VPM model. H.C. gratefully acknowledges the China Scholarship Council for the financial support for a 12-month research at the University of Oklahoma.

References

Aber, J.D., Reich, P.B., Goulden, M.L., 1996. Extrapolating leaf CO_2 exchange to the canopy: a generalized model of forest photosynthesis compared with measurements by eddy correlation. Oecologia 106, 257–265.

Alberto, M.C.R., Wassmann, R., Hirano, T., Miyata, A., Kumar, A., Padre, A., Amante, M., 2009. CO_2/heat fluxes in rice fields: comparative assessment of flooded and non-flooded fields in the Philippines. Agr Forest Meteorol 149, 1737–1750.

Aubinet, M., Grelle, A., Ibrom, A., Rannik, U., Moncrieff, J., Foken, T., Kowalski, A.S., Martin, P.H., Berbigier, P., Bernhofer, C., Clement, R., Elbers, J., Granier, A., Grunwald, T., Morgenstern, K., Pilegaard, K., Rebmann, C., Snijders, W., Valentini, R., Vesala, T., 2000. Estimates of the annual net carbon and water exchange of forests: the EUROFLUX methodology. Adv. Ecol. Res. 30 (30), 113–175.

Baldocchi, D., Falge, E., Gu, L.H., Olson, R., Hollinger, D., Running, S., Anthoni, P., Bernhofer, C., Davis, K., Evans, R., Fuentes, J., Goldstein, A., Katul, G., Law, B., Lee, X.H., Malhi, Y., Meyers, T., Munger, W., Oechel, W., U, K.T.P., Pilegaard, K, Schmid, H.P., Valentini, R., Verma, S., Vesala, T., Wilson, K., Wofsy, S., 2001. FLUXNET: a new tool to study the temporal and spatial variability of ecosystem-scale carbon dioxide, water vapor, and energy flux densities. B Am Meteorol Soc 82, 2415–2434.

Baldocchi, D., Sturtevant, C., Fluxnet, C., 2015. Does day and night sampling reduce spurious correlation between canopy photosynthesis and ecosystem respiration? Agr Forest Meteorol 207, 117–126.

Barton, C.V.M., North, P.R.J., 2001. Remote sensing of canopy light use efficiency using the photochemical reflectance index - Model and sensitivity analysis. Remote Sens Environ 78, 264–273.

Bhattacharyya, P., Neogi, S., Roy, K.S., Dash, P.K., Nayak, A.K., Mohapatra, T., 2014. Tropical low land rice ecosystem is a net carbon sink. Agr Ecosyst Environ 189, 127–135.

Boschetti, M., Busetto, L., Manfron, G., Laborte, A., Asilo, S., Pazhanivelan, S., Nelson, A., 2017. PhenoRice: a method for automatic extraction of spatio-temporal information on rice crops using satellite data time series. Remote Sens Environ 194, 347–365.

Brogaard, S., Runnstrom, M., Seaquist, J.W., 2005. Primary production of Inner Mongolia, China, between 1982 and 1999 estimated by a satellite data-driven light use efficiency model. Glob Planet Change 45, 313–332.

Cai, W., Yuan, W., Liang, S., Liu, S., Dong, W., Chen, Y., Liu, D., Zhang, H., 2014. Large differences in terrestrial vegetation production derived from satellite-based light use efficiency models. Remote Sens-Basel 6, 8945–8965.

Campbell, C.S., Heilman, J.L., McInnes, K.J., Wilson, L.T., Medley, J.C., Wu, G.W., Cobos, D.R., 2001. Seasonal variation in radiation used efficiency of irrigated rice. Agr Forest Meteorol 110, 45–54.

Chen, J., Jonsson, P., Tamura, M., Gu, Z.H., Matsushita, B., Eklundh, L., 2004. A simple method for reconstructing a high-quality NDVI time-series data set based on the Savitzky-Golay filter. Remote Sens Environ 91, 332–344.

Chen, T., van der Werf, G.R., Dolman, A.J., Groenendijk, M., 2011. Evaluation of cropland maximum light use efficiency using eddy flux measurements in North America and Europe. Geophys Res Lett 38.

Cheng, Y.-.B., Zhang, Q., Lyapustin, A.I., Wang, Y., Middleton, E.M., 2014. Impacts of light use efficiency and fPAR parameterization on gross primary production modeling. Agr Forest Meteorol 189, 187–197.

Choi, J., Ko, J., Ng, C.T., Jeong, S., Tenhunen, J., Xue, W., Cho, J., 2018. Quantification of CO_2 fluxes in paddy rice based on the characterization and simulation of CO_2 assimilation approaches. Agr Forest Meteorol 249, 348–366.

Dye, D.G., 2004. Spectral composition and quanta-to-energy ratio of diffuse photosynthetically active radiation under diverse cloud conditions. J Geophys Res-Atmos 109, D10203.

Falge, E., Baldocchi, D., Olson, R., Anthoni, P., Aubinet, M., Bernhofer, C., Burba, G., Ceulemans, R., Clement, R., Dolman, H., Granier, A., Gross, P., Grunwald, T., Hollinger, D., Jensen, N.O., Katul, G., Keronen, P., Kowalski, A., Lai, C.T., Law, B.E., Meyers, T., Moncrieff, H., Moors, E., Munger, J.W., Pilegaard, K., Rannik, U., Rebmann, C., Suyker, A., Tenhunen, J., Tu, K., Verma, S., Vesala, T., Wilson, K., Wofsy, S., 2001. Gap filling strategies for defensible annual sums of net ecosystem exchange. Agr Forest Meteorol 107, 43–69.

FAOSTAT, 2017. Statistical Database of the Food and Agricultural Organization of the United Nations.

Field, C.B., Randerson, J.T., Malmstrom, C.M., 1995. GLOBAL NET PRIMARY PRODUCTION - COMBINING ECOLOGY AND REMOTE-SENSING. Remote Sens Environ 51, 74–88.

Foken, T., Wichura, B., 1996. Tools for quality assessment of surface-based flux measurements. Agr Forest Meteorol 78, 83–105.

Fu, G., Zhang, J., Shen, Z.-.X., Shi, P.-.L., He, Y.-.T., Zhang, X.-.Z., 2017. Validation of collection of 6 MODIS/Terra and MODIS/Aqua gross primary production in an alpine meadow of the Northern Tibetan Plateau. Int J Remote Sens 38, 4517–4534.

Gitelson, A.A., Peng, Y., Arkebauer, T.J., Schepers, J., 2014. Relationships between gross primary production, green LAI, and canopy chlorophyll content in maize: implications for remote sensing of primary production. Remote Sens Environ 144, 65–72.

Hanan, N.P., Burba, G., Verma, S.B., Berry, J.A., Suyker, A., Walter-Shea, E.A., 2002. Inversion of net ecosystem CO_2 flux measurements for estimation of canopy PAR absorption. Global Change Biol. 8, 563–574.

Hatala, J.A., Detto, M., Sonnentag, O., Deverel, S.J., Verfaillie, J., Baldocchi, D.D., 2012. Greenhouse gas (CO_2, CH_4, H_2O) fluxes from drained and flooded agricultural peatlands in the Sacramento-San Joaquin Delta. Agr Ecosyst Environ. 150, 1–18.

He, H., Liu, M., Xiao, X., Ren, X., Zhang, L., Sun, X., Yang, Y., Li, Y., Zhao, L., Shi, P., Du, M., Ma, Y., Ma, M., Zhang, Y., Yu, G., 2014. Large-scale estimation and uncertainty analysis of gross primary production in Tibetan alpine grasslands. J Geophys Res-Biogeo 119, 466–486.

Hong, J.K., Kwon, H.J., Lim, J.H., H., B.Y., Lee, J.H., Kim, J., 2009. Standardization of KoFlux Eddy-Covariance Data Processing. Korean J. Agric. Forest Meteorol. 11, 19–26.

Huete, A., Didan, K., Miura, T., Rodriguez, E.P., Gao, X., Ferreira, L.G., 2002. Overview of the radiometric and biophysical performance of the MODIS vegetation indices. Remote Sens Environ 83, 195–213.
Huete, A.R., Liu, H.Q., Batchily, K., vanLeeuwen, W., 1997. A comparison of vegetation indices global set of TM images for EOS-MODIS. Remote Sens Environ 59, 440–451.
Hwang, Y., Ryu, Y., Huang, Y., Kim, J., Iwata, H., Kang, M., 2020. Comprehensive assessments of carbon dynamics in an intermittently-irrigated rice paddy. Agr Forest Meteorol 285.
Inoue, Y., Penuelas, J., Miyata, A., Mano, M., 2008. Normalized difference spectral indices for estimating photosynthetic efficiency and capacity at a canopy scale derived from hyperspectral and CO_2 flux measurements in rice. Remote Sens Environ 112, 156–172.
Jin, C., Xiao, X., Merbold, L., Arneth, A., Veenendaal, E., Kutsch, W.L., 2013. Phenology and gross primary production of two dominant savanna woodland ecosystems in Southern Africa. Remote Sens Environ 135, 189–201.
Kiniry, J.R., McCauley, G., Xie, Y., Arnold, J.G., 2001. Rice parameters describing crop performance of four US cultivars. Agron J 93, 1354–1361.
Knox, S.H., Matthes, J.H., Sturtevant, C., Oikawa, P.Y., Verfaillie, J., Baldocchi, D., 2016. Biophysical controls on interannual variability in ecosystem-scale CO_2 and CH_4 exchange in a California rice paddy. J Geophys Res-Biogeo 121, 978–1001.
Knox, S.H., Sturtevant, C., Matthes, J.H., Koteen, L., Verfaillie, J., Baldocchi, D., 2015. Agricultural peatland restoration: effects of land-use change on greenhouse gas (CO_2 and CH_4) fluxes in the Sacramento-San Joaquin Delta. Global Change Biol 21, 750–765.
Kwon, H., Kim, J., Hong, J., Lim, J.H., 2010. Influence of the Asian monsoon on net ecosystem carbon exchange in two major ecosystems in Korea. Biogeosciences 7, 1493–1504.
Lee, B., Kwon, H., Miyata, A., Lindner, S., Tenhunen, J., 2017. Evaluation of a Phenology-Dependent Response Method for Estimating Leaf Area Index of Rice Across Climate Gradients. Remote Sens-Basel, 9.
Lindner, S., Xue, W., Nay-Htoon, B., Choi, J., Ege, Y., Lichtenwald, N., Fischer, F., Ko, J., Tenhunen, J., Otieno, D., 2016. Canopy scale CO_2 exchange and productivity of transplanted paddy and direct seeded rainfed rice production systems in S Korea. Agr Forest Meteorol 228, 229–238.
Liu, Y., Wan, K.-y., Tao, Y., Li, Z.-g., Zhang, G.-s., Li, S.-l., Chen, F., 2013. Carbon dioxide flux from rice paddy soils in central china: effects of intermittent flooding and draining cycles. PLoS ONE 8 (2), e56562.
Ma, J.N., Zhang, C., Yun, W.J., Lv, Y.H., Chen, W.L., Zhu, D.H., 2020. The temporal analysis of regional cultivated land productivity with GPP Based on 2000-2018 MODIS Data. Sustainability-Basel 12 (1), 411.
Machwitz, M., Gessner, U., Conrad, C., Falk, U., Richters, J., Dech, S., 2015. Modelling the gross primary productivity of West Africa with the regional biomass Model RBM plus, using optimized 250 m MODIS FPAR and fractional vegetation cover information. Int J Appl Earth Obs 43, 177–194.
Meek, D.W., Hatfield, J.L., Howell, T.A., Idso, S.B., Reginato, R.J., 1984. A Generalized relationship between photosynthetically active radiation and solar-radiation. Agron J 76, 939–945.
Monteith, J.L., 1972. Solar-radiation and productivity in tropical ecosystems. J Appl Ecol 9, 747–766.
Monteith, J.L., 1977. Climate and efficiency of crop production in Britain. Philos. Trans. R Soc. Lond Biol Sci. 281, 277–294.
Neue, H.U., 1993. Methane emission from rice fields. Bioscience 43, 466–474.
Nichol, C.J., Huemmrich, K.F., Black, T.A., Jarvis, P.G., Walthall, C.L., Grace, J., Hall, F. G., 2000. Remote sensing of photosynthetic-light-use efficiency of boreal forest. Agr Forest Meteorol 101, 131–142.
Ono, K., Mano, M., Han, G.H., Nagai, H., Yamada, T., Kobayashi, Y., Miyata, A., Inoue, Y., Lal, R., 2015. Environmental controls on fallow carbon dioxide flux in a single-crop rice paddy, Japan. Land Degradation Dev. 26, 331–339.
Pan, G.X., Li, L.Q., Wu, L.S., Zhang, X.H., 2004. Storage and sequestration potential of topsoil organic carbon in China`s paddy soils. Global Change Biol 10, 79–92.
P., D., Blanken, 1998. Turbulent flux measurements above and below the overstory of a boreal aspen forest. Boundary Layer Meteorol.
Pei, Y., Huang, J., Wang, L., Chi, H., Zhao, Y., 2018. An improved phenology-based CASA model for estimating net primary production of forest in central China based on Landsat images. Int J Remote Sens 39, 7664–7692.
Potter, C.S., Randerson, J.T., Field, C.B., Matson, P.A., Vitousek, P.M., Mooney, H.A., Klooster, S.A., 1993. Terrestrial ecosystem production - A process model-based on global satellite and surface data. Global Biogeochem. Cy 7, 811–841.
Reichstein, M., Falge, E., Baldocchi, D., Papale, D., Aubinet, M., Berbigier, P., Bernhofer, C., Buchmann, N., Gilmanov, T., Granier, A., 2005. On the separation of net ecosystem exchange into assimilation and ecosystem respiration: review and improved algorithm. Glob Chang Biol 11, 1424–1439.
Running, S.W., Baldocchi, D.D., Turner, D.P., Gower, S.T., Bakwin, P.S., Hibbard, K.A., 1999. A global terrestrial monitoring network integrating tower fluxes, flask sampling, ecosystem modeling and EOS satellite data. Remote Sens Environ 70, 108–127.
Ryu, Y., Kang, S., Moon, S.-K., Kim, J., 2008. Evaluation of land surface radiation balance derived from moderate resolution imaging spectroradiometer (MODIS) over complex terrain and heterogeneous landscape on clear sky days. Agr Forest Meteorol 148, 1538–1552.
Saichuk, K.J., Schultz, B., White, M.L., Hollier, A.C., Stout, J.M., Brown, S., Eric.;, W.P., Reagan, E.T., Groth, E.D., Salassi, M., Oard, H.J., Linscombe, D.S., Dustin.;, H.L., 2009. Louisiana Rice Production Handbook. LSU AgCenter.
Saito, M., Asanuma, J., Miyata, A., 2007. Dual-scale transport of sensible heat and water vapor over a short canopy under unstable conditions. Water Resour Res 43.
Saito, M., Miyata, A., Nagai, H., Yamada, T., 2005. Seasonal variation of carbon dioxide exchange in rice paddy field in Japan. Agr Forest Meteorol 135, 93–109.
Sasai, T., Nakai, S., Setoyama, Y., Ono, K., Kato, S., Mano, M., Murakami, K., Miyata, A., Saigusa, N., Nemani, R.R., Nasahara, K.N., 2012. Analysis of the spatial variation in the net ecosystem production of rice paddy fields using the diagnostic biosphere model. BEAMS. Ecol Model 247, 175–189.
Savitzky, A., Golay, M.J.E., 1964. Smoothing and differentiation of data by simplified least squares procedures. Anal Chem 36 (8), 1627–1639.
Sims, D.A., Rahman, A.F., Cordova, V.D., El-Masri, B.Z., Baldocchi, D.D., Flanagan, L.B., Goldstein, A.H., Hollinger, D.Y., Misson, L., Monson, R.K., Oechel, W.C., Schmid, H. P., Wofsy, S.C., Xu, L., 2006. On the use of MODIS EVI to assess gross primary productivity of North American ecosystems. J Geophys Res-Biogeo 111, G04015.
Stockli, R., Lawrence, D.M., Niu, G.Y., Oleson, K.W., Thornton, P.E., Yang, Z.L., Bonan, G.B., Denning, A.S., Running, S.W., 2008. Use of FLUXNET in the community land model development. J Geophys Res-Biogeo 113, G01025.
Su, R.R., Liu, K.W, Gen, Y.F., Tian, H., Zhou, S.H., Liu, K.Q., 2013. Characteristics of canopy CO_2 flux over paddy ecosystem in Jianghan plain and its influence factors analysis (in Chinese). Resources and Environment in the Yangtze Basin 22, 1214–1220.
Tagesson, T., Ardo, J., Cappelaere, B., Kergoat, L., Abdi, A., Horion, S., Fensholt, R., 2017. Modelling spatial and temporal dynamics of gross primary production in the Sahel from earth-observation-based photosynthetic capacity and quantum efficiency. Biogeosciences 14, 1333–1348.
Verbesselt, J., Hyndman, R., Zeileis, A., Culvenor, D., 2010. Phenological change detection while accounting for abrupt and gradual trends in satellite image time series. Remote Sens Environ 114, 2970–2980.
Wang, L., Zhu, H., Lin, A., Zou, L., Qin, W., Du, Q., 2017. Evaluation of the Latest MODIS GPP Products Across Multiple Biomes Using Global Eddy Covariance Flux Data. Remote Sens-Basel, 9.
Wang, X., Wu, C., 2019. Estimating the peak of growing season (POS) of China's terrestrial ecosystems. Agr Forest Meteorol 278, 107639.
Wang, Z., Xiao, X.M., Yan, X.D., 2010. Modeling gross primary production of maize cropland and degraded grassland in northeastern China. Agr Forest Meteorol 150, 1160–1167.
White, K., Pontius, J., Schaberg, P., 2014. Remote sensing of spring phenology in northeastern forests: a comparison of methods, field metrics and sources of uncertainty. Remote Sens Environ 148, 97–107.
Williams, M., Richardson, A.D., Reichstein, M., Stoy, P.C., Peylin, P., Verbeeck, H., Carvalhais, N., Jung, M., Hollinger, D.Y., Kattge, J., Leuning, R., Luo, Y., Tomelleri, E., Trudinger, C.M., Wang, Y.P., 2009. Improving land surface models with FLUXNET data. Biogeosciences 6, 1341–1359.
Wu, C., Peng, D., Soudani, K., Siebicke, L., Gough, C.M., Arain, M.A., Bohrer, G., Lafleur, P.M., Peichl, M., Gonsamo, A., Xu, S., Fang, B., Ge, Q., 2017. Land surface phenology derived from normalized difference vegetation index (NDVI) at global FLUXNET sites. Agr Forest Meteorol 233, 171–182.
Wu, C.Y., Niu, Z., Gao, S.A., 2010. Gross primary production estimation from MODIS data with vegetation index and photosynthetically active radiation in maize. J Geophys Res-Atmos 115, D12127.
Wu, X.C., Xiao, X.M., Zhang, Y., He, W., Wolf, S., Chen, J.Q., He, M.Z., Gough, C.M., Qin, Y.W., Zhou, Y.L., Doughty, R., Blanken, P.D., 2018. Spatiotemporal Consistency of four gross primary production products and solar-induced chlorophyll fluorescence in response to climate extremes across CONUS in 2012. J Geophys Res-Biogeo 123, 3140–3161.
Xiao, J., Davis, K.J., Urban, N.M., Keller, K., Saliendra, N.Z., 2011. Upscaling carbon fluxes from towers to the regional scale: influence of parameter variability and land cover representation on regional flux estimates. J Geophys Res-Biogeo 116, G00J06.
Xiao, X.M., Braswell, B., Zhang, Q.Y., Boles, S., Frolking, S., Moore, B., 2003. Sensitivity of vegetation indices to atmospheric aerosols: continental-scale observations in Northern Asia. Remote Sens Environ 84, 385–392.
Xiao, X.M., Hollinger, D., Aber, J., Goltz, M., Davidson, E.A., Zhang, Q.Y., Moore, B., 2004a. Satellite-based modeling of gross primary production in an evergreen needleleaf forest. Remote Sens Environ 89, 519–534.
Xiao, X.M., Zhang, Q.Y., Braswell, B., Urbanski, S., Boles, S., Wofsy, S., Berrien, M., Ojima, D., 2004b. Modeling gross primary production of temperate deciduous broadleaf forest using satellite images and climate data. Remote Sens Environ 91, 256–270.
Xiao, X.M., Zhang, Q.Y., Hollinger, D., Aber, J., Moore, B., 2005a. Modeling gross primary production of an evergreen needleleaf forest using modis and climate data. Ecol Appl 15, 954–969.
Xiao, X.M., Zhang, Q.Y., Saleska, S., Hutyra, L., De Camargo, P., Wofsy, S., Frolking, S., Boles, S., Keller, M., Moore, B., 2005b. Satellite-based modeling of gross primary production in a seasonally moist tropical evergreen forest. Remote Sens Environ 94, 105–122.
Xin, F.F., Xiao, X.M., Zhao, B., Miyata, A., Baldocchi, D., Knox, S., Kang, M., Shim, K.M., Min, S., Chen, B.Q., Li, X.P., Wang, J., Dong, J.W., Biradar, C., 2017. Modeling gross primary production of paddy rice cropland through analyses of data from CO_2 eddy flux tower sites and MODIS images. Remote Sens Environ 190, 42–55.
Xue, W., Lindner, S., Nay-Htoon, B., Dubbert, M., Otieno, D., Ko, J., Muraoka, H., Werner, C., Tenhunen, J., Harley, P., 2016. Nutritional and developmental influences on components of rice crop light use efficiency. Agr Forest Meteorol 223, 1–16.
Yamori, W., Hikosaka, K., Way, D.A., 2014. Temperature response of photosynthesis in C3, C4, and CAM plants: temperature acclimation and temperature adaptation. Photosynth Res 119, 101–117.

Yan, H., Fu, Y., Xiao, X., Huang, H.Q., He, H., Ediger, L., 2009. Modeling gross primary productivity for winter wheat-maize double cropping System using MODIS time series and CO_2 eddy flux tower data. Agr Ecosyst Environ 129, 391–400.

Yang, J.L., Dong, J.W., Xiao, X.M., Dai, J.H., Wu, C.Y., Xia, J.Y., Zhao, G.S., Zhao, M.M., Li, Z.L., Zhang, Y., Ge, Q.S., 2019. Divergent shifts in peak photosynthesis timing of temperate and alpine grasslands in China. Remote Sens Environ 233, 111395.

Yang, K., Ryu, Y., Dechant, B., Berry, J.A., Hwang, Y., Jiang, C., Kang, M., Min, J., Kimm, H., Kornfeld, A., Yang, X., 2018. Sun-induced chlorophyll fluorescence is more strongly related to absorbed light than to photosynthesis at half-hourly resolution in a rice paddy. Remote Sens Environ 216, 658–673.

Yuan, W., Cai, W., Xia, J., Chen, J., Liu, S., Dong, W., Merbold, L., Law, B., Arain, A., Beringer, J., Bernhofer, C., Black, A., Blanken, P.D., Cescatti, A., Chen, Y., Francois, L., Gianelle, D., Janssens, I.A., Jung, M., Kato, T., Kiely, G., Liu, D., Marcolla, B., Montagnani, L., Raschi, A., Roupsard, O., Varlagin, A., Wohlfahrt, G., 2014. Global comparison of light use efficiency models for simulating terrestrial vegetation gross primary production based on the La Thuile database. Agr Forest Meteorol 192, 108–120.

Yuan, W., Liu, S., Zhou, G., Zhou, G., Tieszen, L.L., Baldocchi, D., Bernhofer, C., Gholz, H., Goldstein, A.H., Goulden, M.L., Hollinger, D.Y., Hu, Y., Law, B.E., Stoy, P. C., Vesala, T., Wofsy, S.C., AmeriFlux, C., 2007. Deriving a light use efficiency model from eddy covariance flux data for predicting daily gross primary production across biomes. Agr Forest Meteorol 143, 189–207.

Zhang, Q., Cheng, Y.-B., Lyapustin, A.I., Wang, Y., Gao, F., Suyker, A., Verma, S., Middleton, E.M., 2014. Estimation of crop gross primary production (GPP): fAPAR (chl) versus MOD15A2 FPAR. Remote Sens Environ 153, 1–6.

Zhang, Q., Middleton, E.M., Margolis, H.A., Drolet, G.G., Barr, A.A., Black, T.A., 2009. Can a satellite-derived estimate of the fraction of PAR absorbed by chlorophyll (FAPAR(chl)) improve predictions of light-use efficiency and ecosystem photosynthesis for a boreal aspen forest? Remote Sens Environ 113, 880–888.

Zhang, Q., Xiao, X., Braswell, B., Linder, E., Ollinger, S., Smith, M.-L., Jenkins, J.P., Baret, F., Richardson, A.D., Moore III, B., Minocha, R., 2006. Characterization of seasonal variation of forest canopy in a temperate deciduous broadleaf forest, using daily MODIS data. Remote Sens Environ 105, 189–203.

Zhang, X.Y., Friedl, M.A., Schaaf, C.B., Strahler, A.H., 2004. Climate controls on vegetation phenological patterns in northern mid- and high latitudes inferred from MODIS data. Global Change Biol 10, 1133–1145.

Zhang, X.Y., Friedl, M.A., Schaaf, C.B., Strahler, A.H., Hodges, J.C.F., Gao, F., Reed, B.C., Huete, A., 2003. Monitoring vegetation phenology using MODIS. Remote Sens Environ 84, 471–475.

Zhang, Y., Xiao, X., Jin, C., Dong, J., Zhou, S., Wagle, P., Joiner, J., Guanter, L., Zhang, Y., Zhang, G., Qin, Y., Wang, J., Moore, B., 2016. Consistency between sun-induced chlorophyll fluorescence and gross primary production of vegetation in North America. Remote Sens Environ 183, 154–169.

Zhang, Y., Xiao, X., Wu, X., Zhou, S., Zhang, G., Qin, Y., Dong, J., 2017. Data Descriptor: a global moderate resolution dataset of gross primary production of vegetation for 2000-2016. Sci Data 4, 170165.

Zhao, M.S., Heinsch, F.A., Nemani, R.R., Running, S.W., 2005. Improvements of the MODIS terrestrial gross and net primary production global data set. Remote Sens Environ 95, 164–176.